

Supporting Information

Novel CO₂-Philic Porous Organic Polymers Synthesised in Water: A Leap towards Eco-Sustainability

Riccardo Mobili,^{a,‡} Yue Wub,^b Charl Xavier Bezuidenhout,^c Sonia La Cognata,^a Silvia Bracco^{c*},
Mariolino Carta^{b*} and Valeria Amendola^{a*}

Index

1. Materials and Methods	S2
2. Synthesis	S5
3. Physicochemical characterization of POPs	S8
4. Gas adsorption studies	S27
5. References	S42

^a Department of Chemistry, University of Pavia
viale Tarquato Taramelli 12, Pavia, 27100, Italy
e-mail: valeria.amendola@unipv.it

^b Department of Chemistry, Faculty of
Science and Engineering, Swansea University
Singleton Park, Swansea, Wales, SA2 8PP (UK)
e-mail: mariolino.carta@swansea.ac.uk

^c Department of Materials Science, University of Milano-Bicocca
Via Cozzi 55, Milano, 20125, Italy

‡ present address: Sorbonne Université, CNRS, Institut Parisien de Chimie Moléculaire, 4 Place Jussieu, 75005 Paris, France

1. Materials and Methods

All commercially available starting materials, including 1,3,5-tris(bromomethyl)-2,4,6-triethylbenzene ($\geq 98\%$), 1,3,5-tris(bromomethyl)-mesitylene ($\geq 98\%$), phloroglucinol dihydrate ($\geq 99\%$) and HPLC grade solvents, were purchased from Merck, Sigma-Aldrich and VWR and used without further purification. 1,3,5-tris(methylamino)-2,4,6-triethylbenzene (EtNH_2), 1,3,5-tris(methylamino)-mesitylene (MeNH_2) and triformylphloroglucinol (TFP) were synthesized following already known procedures,^{S1-S3} starting from purchasable compounds. The polymers syntheses were conducted in WHEATON® liquid scintillation vials (Sigma-Aldrich) closed with a screw cap (capacity: 20 mL); the reaction conditions were not controlled to exclude moisture or oxygen.

Characterization spectra obtained for EtNH_2 , MeNH_2 and TFP were in line with those reported in the literature. $^1\text{H-NMR}$ spectra were recorded on a Bruker AVANCEIII 400 MHz (operating at 9.37 T, 400 MHz), equipped with a 5 mm BBO probe head with Z-gradient (Bruker BioSpin). Deuterated solvents used for NMR analysis were purchased and used as received. Chemical shifts are reported in ppm with the residual solvent as internal reference. The data were processed with Topspin 4.1 (Bruker Biospin). Elemental analyses were conducted on a Perkin Elmer CHN 2400SERIES II ELEMENTAL ANALYZER at the Department of Chemistry of the University of Milano (Italy).

For the Fourier Transform – Infrared analysis (FT-IR), a Nicolet FT-IR iS10 spectrometer (Nicolet, Madison, WI, USA) equipped with attenuated total reflectance (ATR) sampling accessory (Smart iTR with diamond plate) was used. Thirty-two scans in the $4000\text{--}600\text{ cm}^{-1}$ range at 4 cm^{-1} resolution were co-added. Well-ground powder samples were used, and spectra were obtained after pressing the sample onto an ATR diamond crystal at room temperature ($20\text{ }^\circ\text{C}$).

Powder x-ray diffraction (PXRD) measurements were performed with a Rigaku Smarlab powder diffractometer using $\text{Cu-K}\alpha$ radiation at 40 kV and 20 mA scanning over a range of $2.0\text{--}80.0^\circ$ 2θ with a step size of 0.01° and a scan speed of $1.5^\circ/\text{min}$. The experiments was performed in air using a 0.2 mm depth sample holder.

Elemental analysis was performed with a vario MICRO Element Analyzer in CHNS mode.

Thermogravimetric analysis (TGA) was performed on a Q5000 apparatus (TA Instruments, New Castle, DE, USA) interfaced with a TA5000 data station under nitrogen flux (10 mL min^{-1}) in a platinum pan by heating about 3 mg of sample from room temperature up to $650 \text{ }^\circ\text{C}$ (heating rate 5 K min^{-1}). TGA data were analyzed by the Universal Analysis software by TA Instruments.

Differential scanning calorimetry (DSC) was performed by a Q2000 apparatus (TA Instruments, New Castle, DE, USA) interfaced with a TA5000 data station by heating about 3 mg of samples in an open aluminium crucible from $-75 \text{ }^\circ\text{C}$ to $350 \text{ }^\circ\text{C}$, cooling down to -75°C and heating up to room temperature (heating and cooling rate = 5 K min^{-1}) under nitrogen flux (50 mL min^{-1}). The temperature accuracy of the instrument is $\pm 0.1 \text{ }^\circ\text{C}$, the precision is $\pm 0.01 \text{ }^\circ\text{C}$, and the calorimetric reproducibility is $\pm 0.05\%$. DSC data were analysed by the Universal Analysis software by TA Instruments.

A Zeiss EVO MA10 (Carl Zeiss, Oberkochen, Germany) Scanning Electron Microscope (SEM) was used for the morphological study on gold sputtered samples (Secondary Electrons detector). The measurements were performed at 20 kV with a working distance of 8.5 mm.

^{13}C and ^1H solid-state NMR experiments were carried out with a Bruker NEO 300 instrument operating at a static field of 7.04 T equipped a 4 mm double resonance MAS probe. $^{13}\text{C}\{^1\text{H}\}$ ramped-amplitude Cross Polarization (CP) experiments were performed at 298 K at a spinning speed of 12.5 kHz using a recycle delay of 5 s and contact times of 2 ms and 50 μs . The 90° pulse for proton was 2.9 ms. ^{13}C SPE MAS spectra were collected with a recycle delay of 60 s. Crystalline polyethylene was taken as an external reference at 32.8 ppm from TMS. Quantitative solid-state ^1H MAS NMR spectra were performed at a spinning speed of 12.5 kHz using a recycle delay of 20 s. The ^1H chemical shift was referenced to adamantane.

For the gas adsorption studies the samples were weighed in a Quantachrome adsorption cell and outgassed under vacuum for 15 hours at 353 K.

N_2 (298 K) and CO_2 (195 K, 273 K and 298 K) adsorption/desorption measurements were made using a Quantachrome Nova-e. Samples were degassed for 800 min at $100 \text{ }^\circ\text{C}$ under high vacuum prior to analysis. The gases were supplied by BOC and used without any further purification (N_2 purity > 99.999 , CO_2 purity $> 99.995\%$). The specimen was measured twice after outgas in two different cells to minimize the error, providing the same results. The data were analysed with the software provided with the instrument. The BET was calculated at a relative pressure $P/P_0 < 0.1$.

NLDFT and H-K analysis were performed to calculate the pore size distribution and volume, considering a carbon equilibrium transition kernel at 273 K based on a slit-pore model; the kernel is based on a common, one centre, Lennard-Jones model. P_0 always refers to 1 bar, which is the maximum pressure reached by the instrument, not the saturation pressure of the probe gas. To assess the potential chemisorption, heats of adsorption were calculated from the CO₂ curves measured at 273K and 298K. The data were analysed with the QuadraWin software and fitted with the Langmuir-Freundlich equation and calculated via the Clausius-Clapeyron equation.

2. Synthesis

The starting amines were prepared following a procedure already known in the literature.^{S1-S3} The synthesis and characterization of 1,3,5-tris(methylamino)-2,4,6-triethylbenzene (EtNH₂) has been reported by our group in a recent work.^{S1} The employed building blocks, EtNH₂, MeNH₂, and TFP, have been characterized by ¹H-NMR (Figures S1-S3) and FTIR (Figures S12-S13), and the obtained spectra corresponded to those reported in the literature for these compounds.^{S1-S3}

2.1 Synthesis of 1,3,5-tris(methylamino)-2,4,6-trimethylbenzene^{S2} (MeNH₂)

Potassium phthalamide (5.84 g, 31.6 mmol, 3.6 eq.) was added to a solution of 1,3,5-tris(bromomethyl)-2,4,6-trimethylbenzene (3.50 g, 8.77 mmol, 1 eq.) and 18-crown-6 (0.69 g, 2.63 mmol, 0.3 eq.) in toluene (30 mL). The mixture was refluxed under nitrogen for about 24 h. The solid residue, collected after concentrating the mixture in vacuo, was suspended in water (50 mL) and collected by filtration. The resulting solid was washed with water (3 × 10 mL) and MeOH (20 mL). After drying in vacuo, the product, *i.e.* 2,2',2''-((2,4,6-Trimethylbenzene-1,3,5-triyl)tris(methylene))tris(isoindoline-1,3-dione), was employed in the second step of the procedure without further purification (4.82 g, 8.07 mmol, yield: 92%).

The obtained compound (4.82 g, 8.07 mmol) was suspended in 60 mL of toluene/MeOH mixture 2:1 (v:v), and then treated with an excess of hydrazine hydrate (3.1 mL, 50 wt% solution in water, 48.4 mmol). After two-days heating at 90°C, the mixture was concentrated in vacuo and treated with aqueous KOH (30 mL, 40 wt%). The aqueous phase was then extracted with CHCl₃ (3 × 50 mL). The collected organic layers were combined and dried over anhydrous Na₂SO₄. After concentrating in vacuo, the desired final triamine compound was collected as a white powder. The product was used without further purification (1.50 g, 7.26 mmol, yield: 90%). ¹H-NMR signals correspond to those reported in literature (see Figure S2). Overall yield: 83%

¹H-NMR (400 MHz, CDCl₃) δ: 3.86 (s, 6H, CH₂N), 2.38 (s, 9H, CH₃).

2.2 Triformylphloroglucinol^{S3}

Phloroglucinol dihydrate (7.96 g, 49 mmol, 1 eq.) and hexamethylenetetramine (15,10 g, 108 mmol, 2.2 eq.) are dissolved in trifluoroacetic acid (90 mL) under N₂. The reaction mixture is heated at 100 °C for 2.5 hours and then HCl 3M is added (150 mL). The heating at 100 °C is maintained for 1 hour and then the reaction is cooled down to room temperature. Stirring is then maintained overnight. After one night the mixture is filtered on a Celite pad and the red solution

is extracted with DCM (4 x 100 mL). The reunited organic phases are dried over Na₂SO₄, filtered and the solvent is removed under vacuum to obtain 1.05 g of a brownish-red solid. The product was used without further purification. Yield: 10.2 %. ¹H-NMR signals correspond to those reported in literature (see Figure S3).

¹H-NMR (400 MHz, CDCl₃) δ: 14.17 (s, 3H, CHO), 10.18 (s, 3H, OH).

2.3 ¹H-NMR characterization of EtNH₂, MeNH₂, TFP

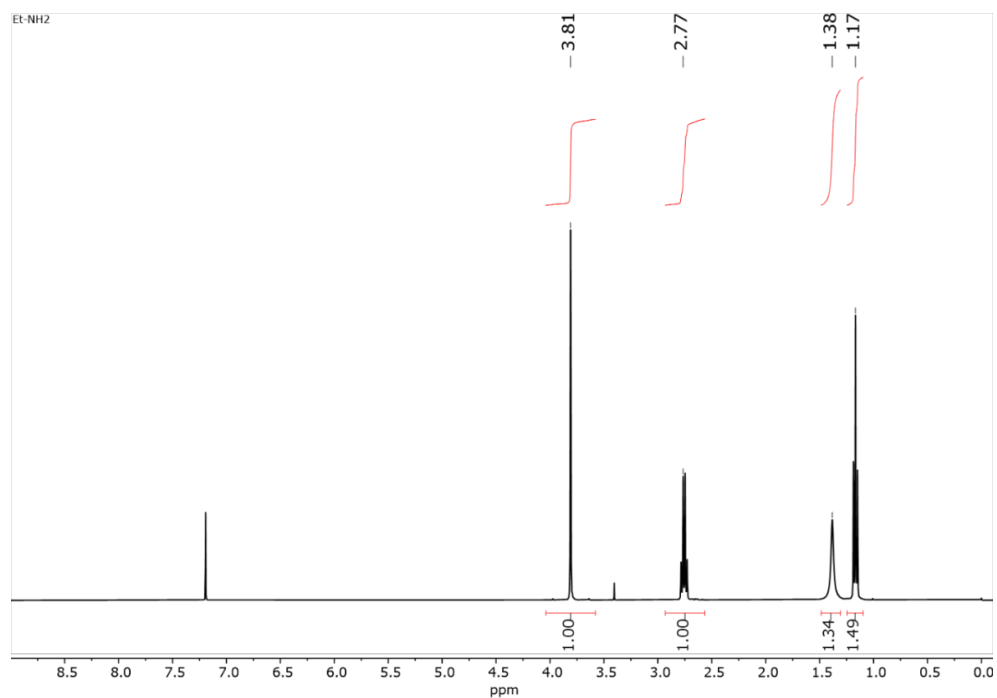


Figure S1. ¹H-NMR (CDCl₃) spectrum of EtNH₂

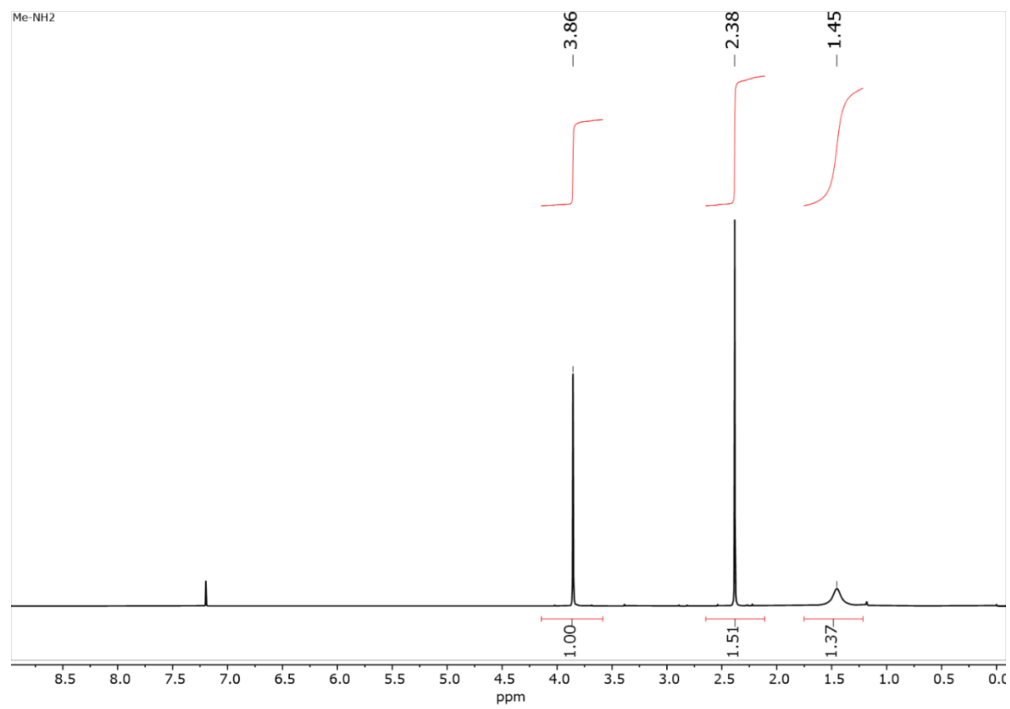


Figure S2. ¹H-NMR (CDCl₃) spectrum of MeNH₂

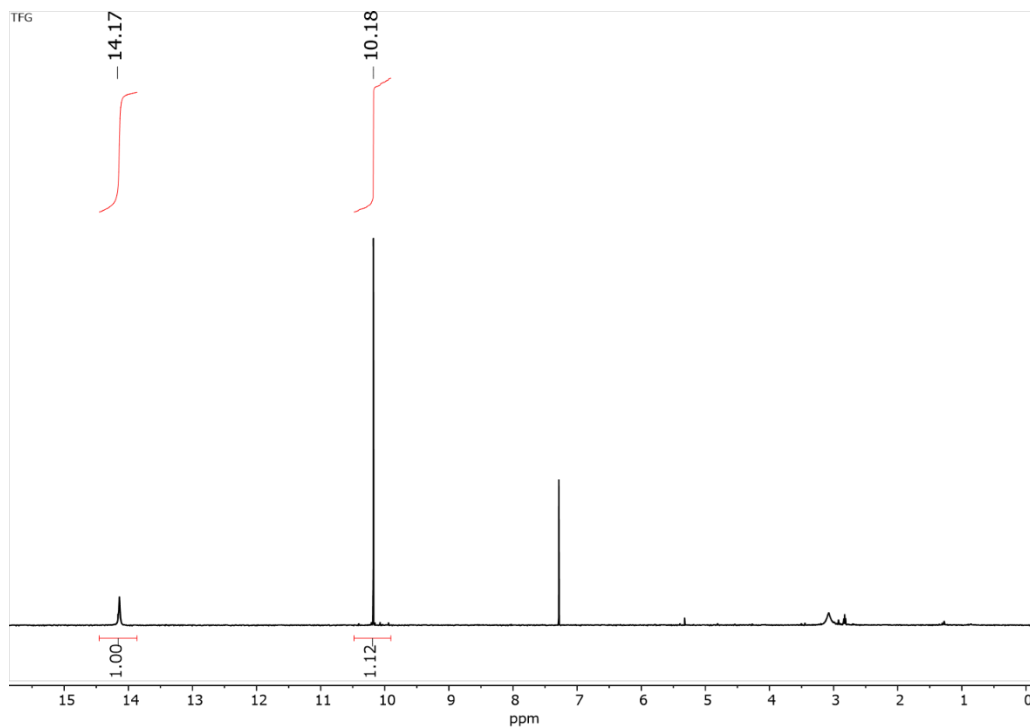


Figure S3. ¹H-NMR (CDCl₃) spectrum of TFP

3. Physicochemical characterization of POPs

3.1 Elemental Analysis

Table S1. Elemental Analysis of POPs. The theoretical percentages are shown in brackets.

Sample	Weight (mg)	C %	H %	N %	S (%)*	C/N atoms
POP-W-Et	2.27	67.58 (71.10)	7.093 (6.71)	10.47 (10.36)	0.124	7.6 (8)
POP-W-Me	2.21	66.66 (69.40)	6.566 (5.83)	11.65 (11.57)	0.017	6.7 (7)
POP-O-Et	3.68	63.46 (71.10)	6.037 (6.71)	8.80 (10.36)	0.098	8.4 (8)
POP-O-Me	2.13	66.05 (69.40)	6.202 (5.83)	10.4 (11.57)	0.103	7.4 (7)

* the sulfur contained in the polymer samples is attributable to an impurity derived from the starting materials.

3.2 Thermogravimetric Analysis

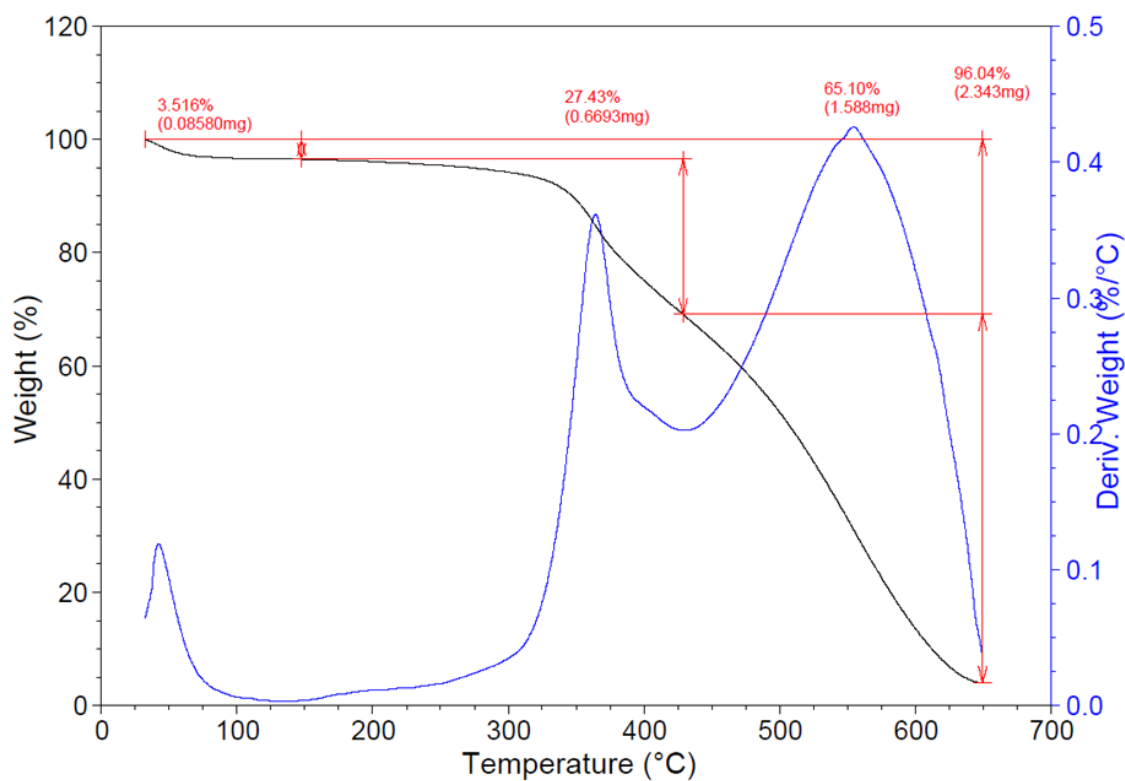


Figure S4 TGA-DTG curves for POP-W-Et

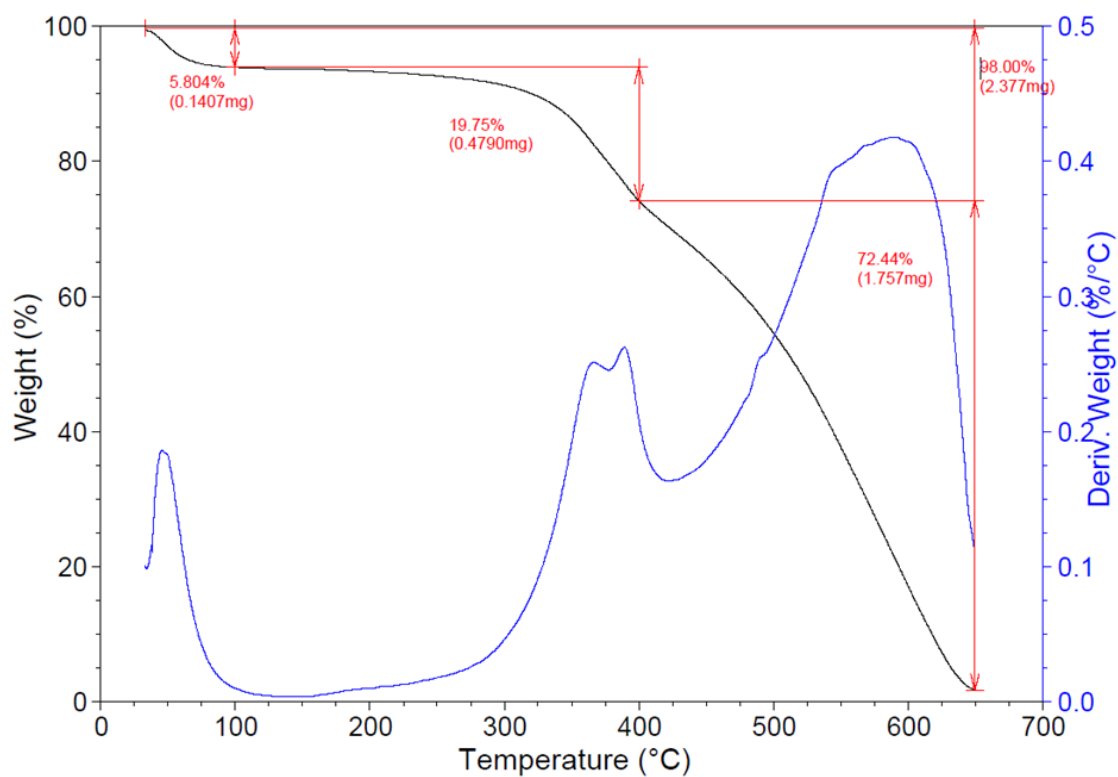


Figure S5 TGA-DTG curves for POP-O-Et

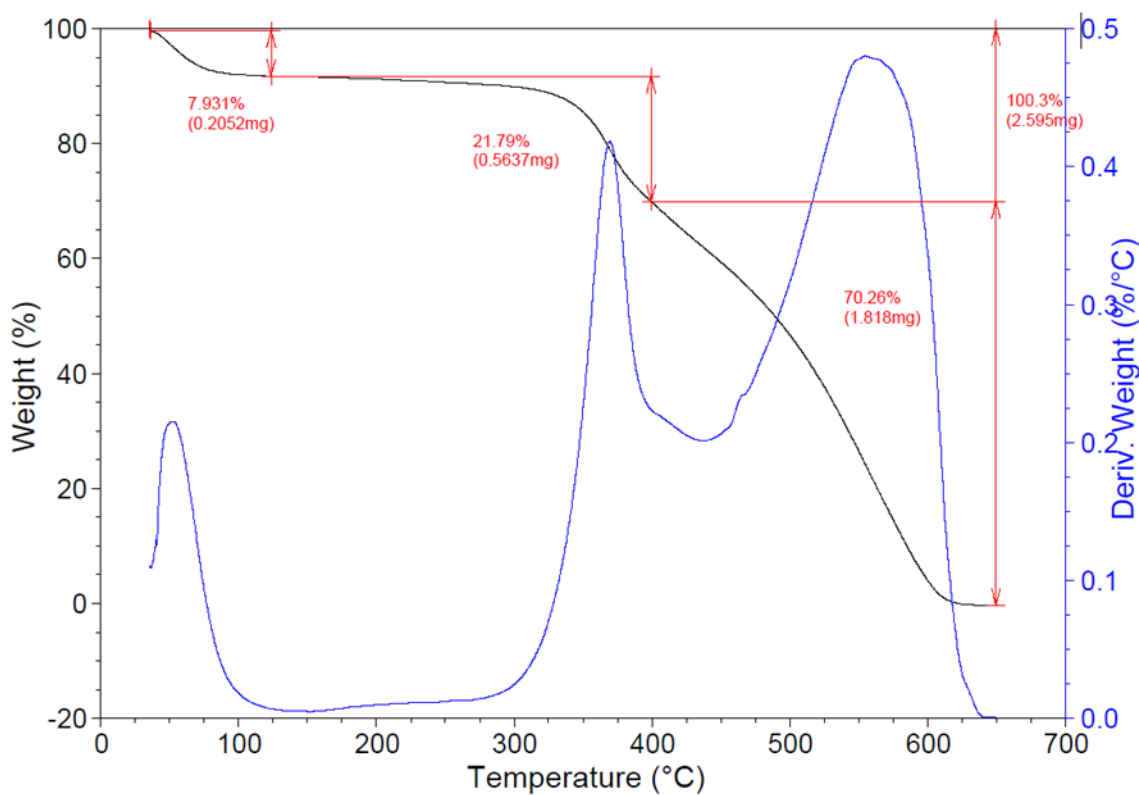


Figure S6 TGA-DTG curves for POP-W-Me

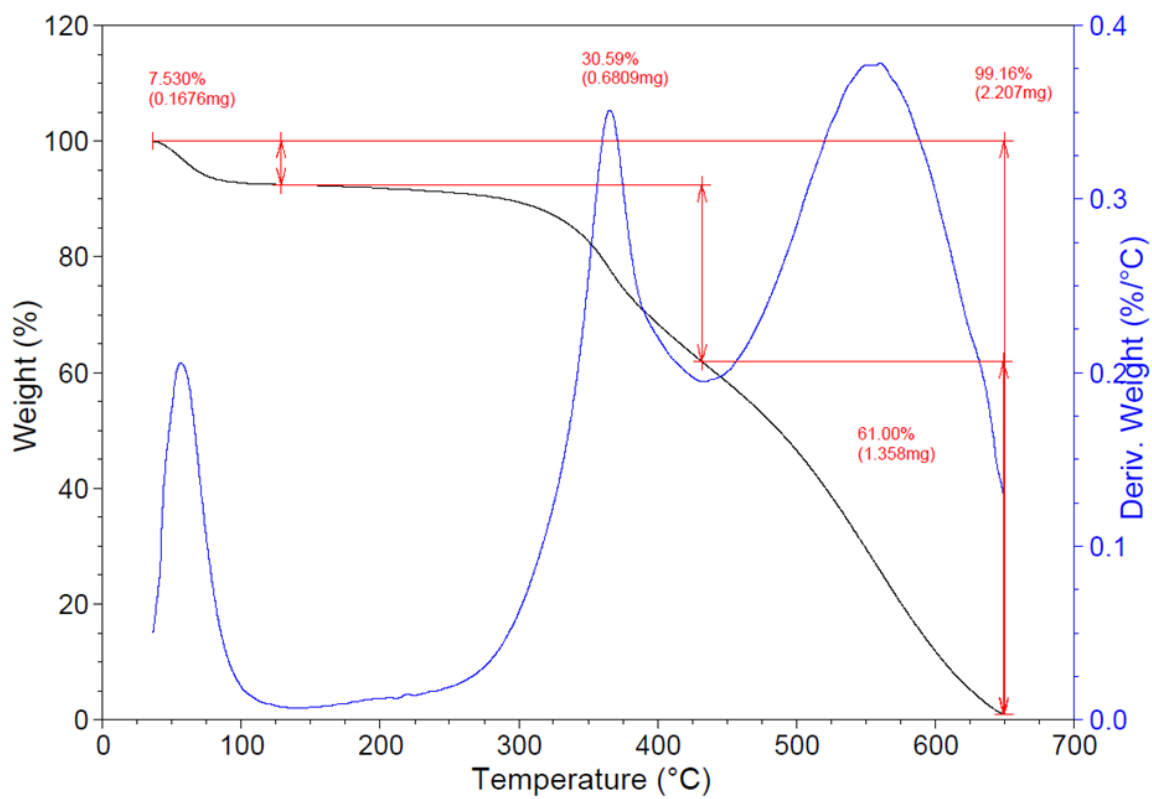


Figure S7 TGA-DTG curves for POP-O-Me

3.3 Differential Scanning Calorimetry Analysis

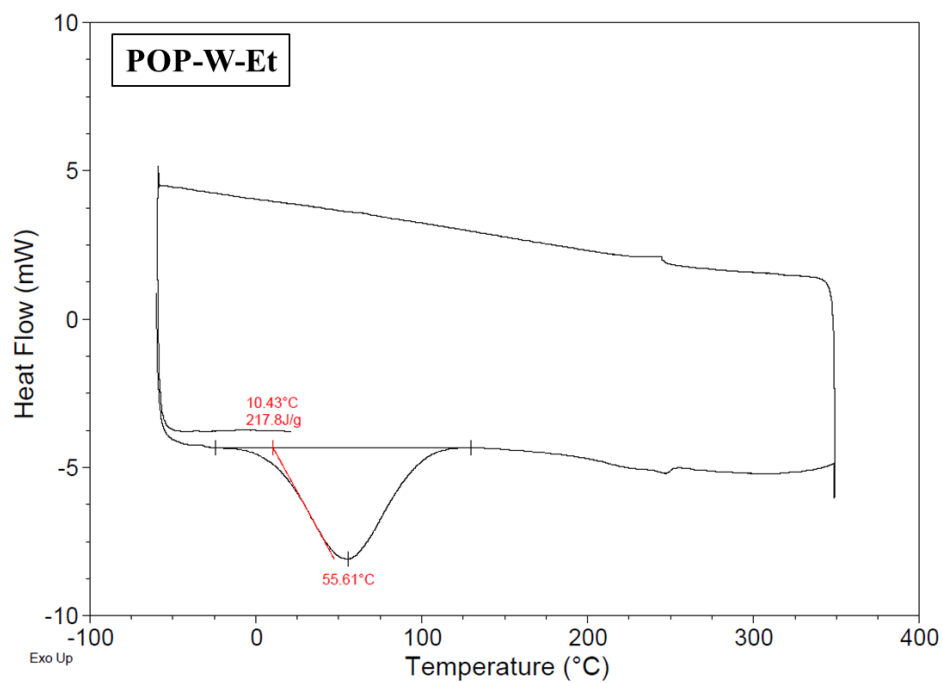


Figure S8 DSC for POP-W-Et

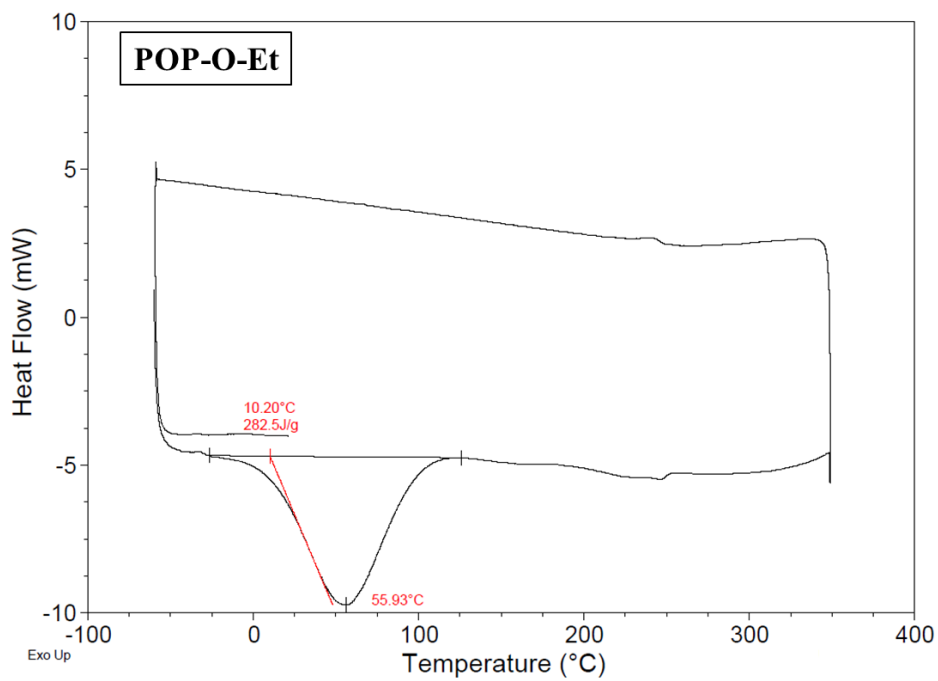


Figure S9 DSC for POP-O-Et

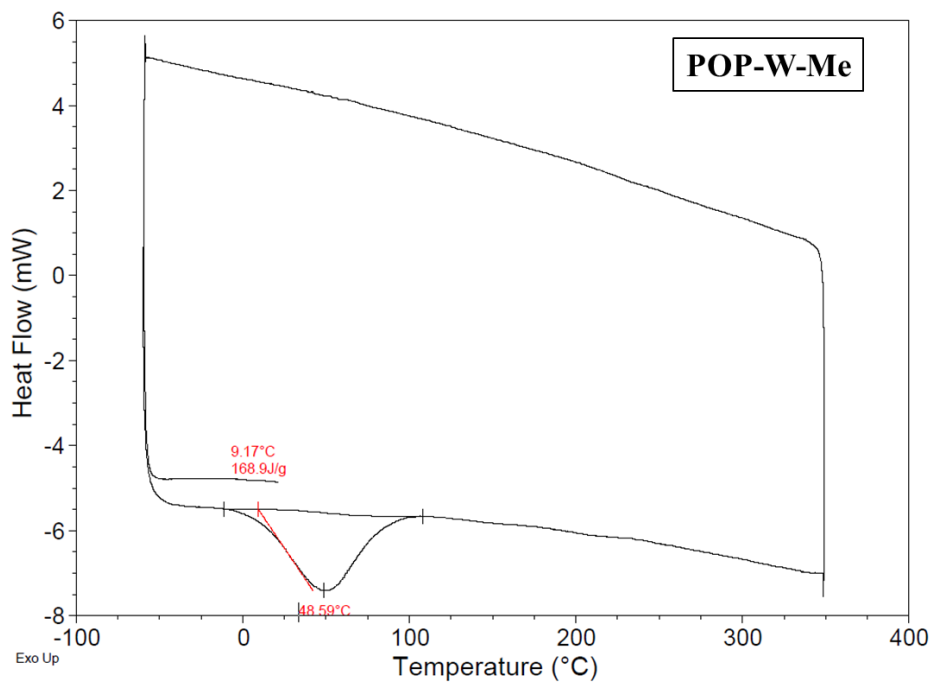


Figure S10 DSC for POP-W-Me

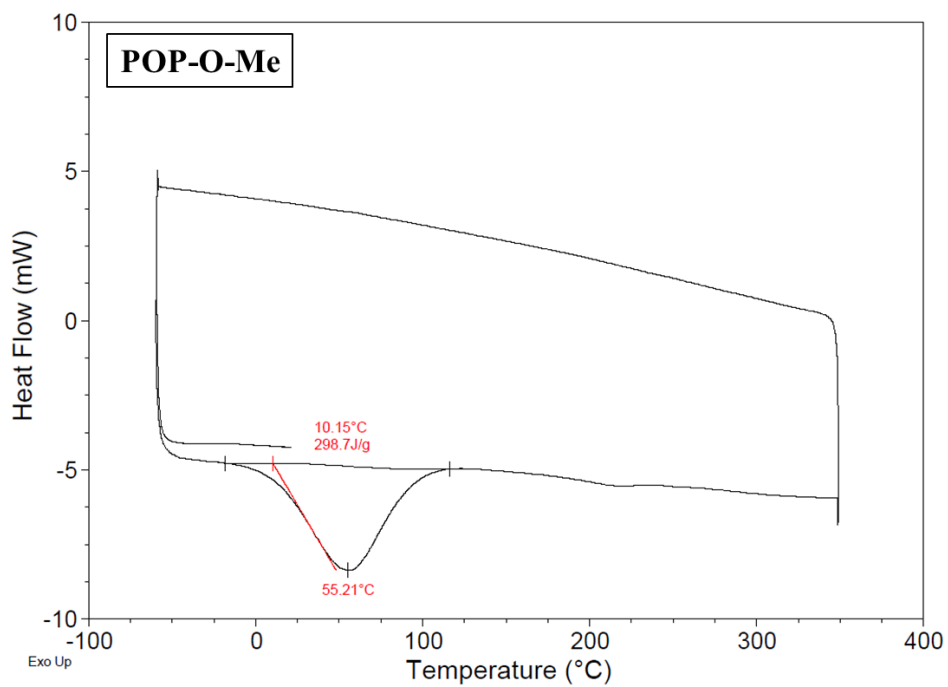


Figure S11 DSC for POP-O-Me

3.4 FT-IR Analysis

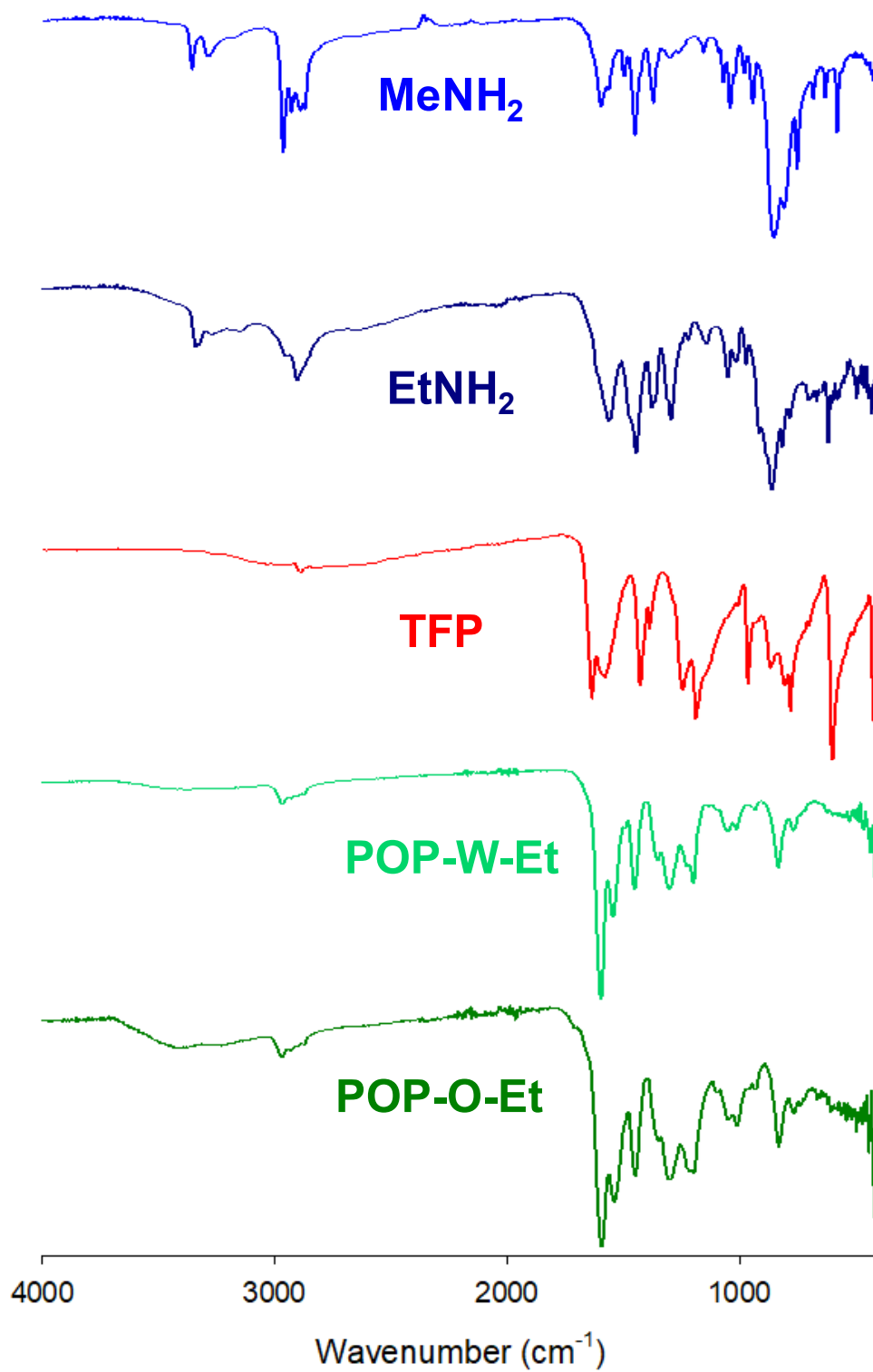


Figure S12. FT-IR spectra of POP-W/O-Et materials and precursors.

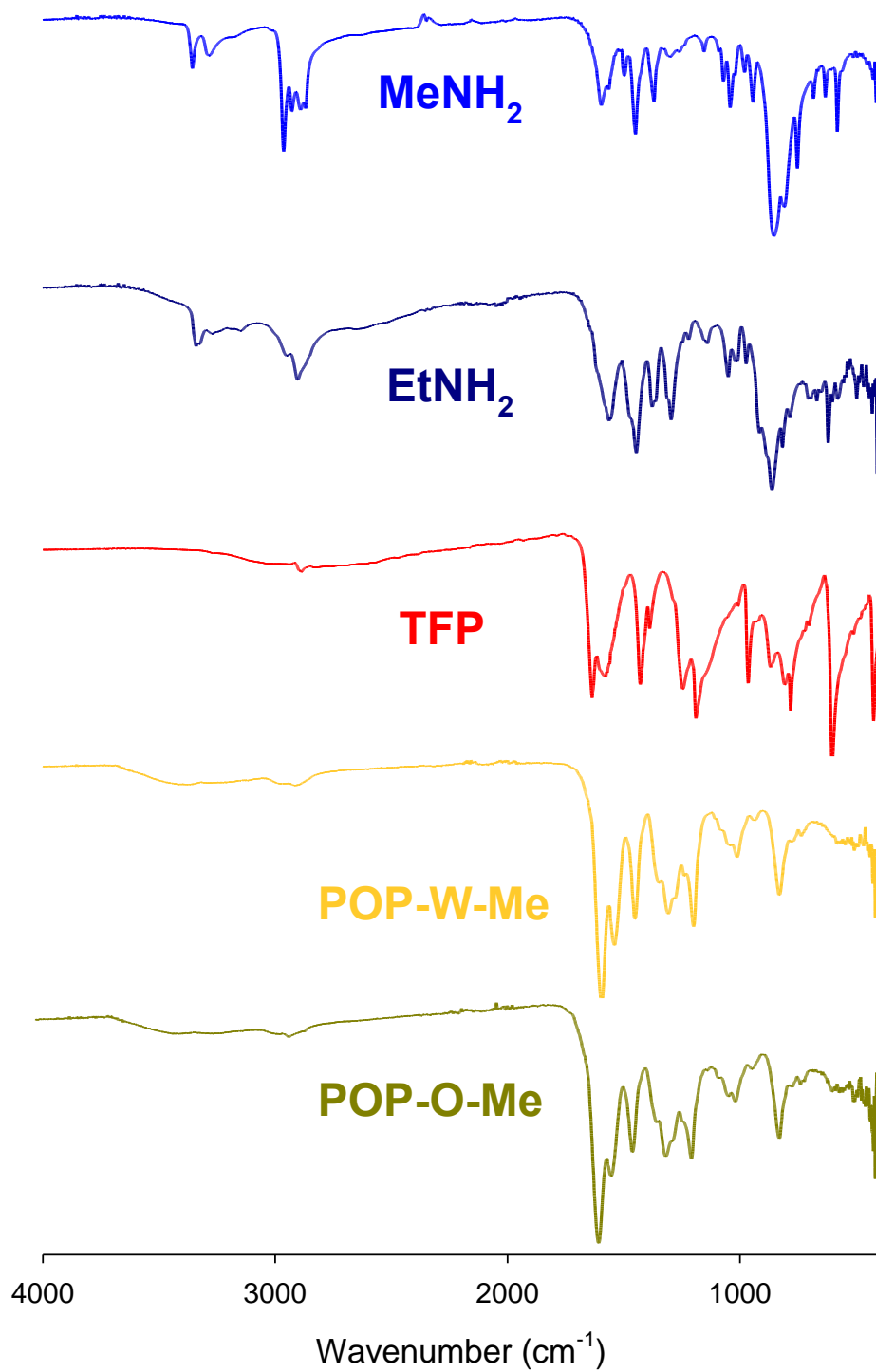


Figure S13. FT-IR spectra of POP-W/O-Me materials and precursors.

3.5 Solid-State NMR

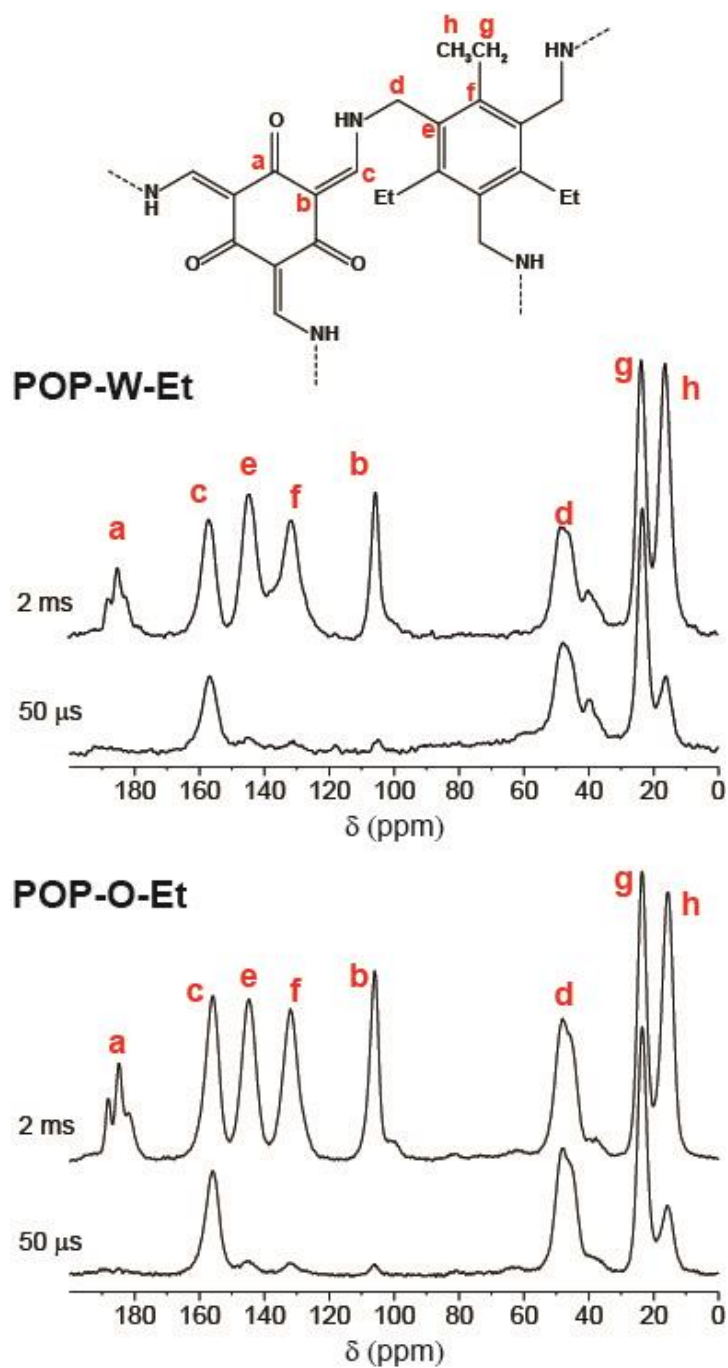


Figure S14. $^{13}\text{C}\{^1\text{H}\}$ CP MAS spectra of **POP-W-Et** and **POP-O-Et** (up and down, respectively) materials performed at 298 K at a spinning speed of 12.5 kHz with contact times of 2 ms and 50 μs . (The samples were treated under high vacuum at 80 $^\circ\text{C}$ for 12 hours before the NMR measurements).

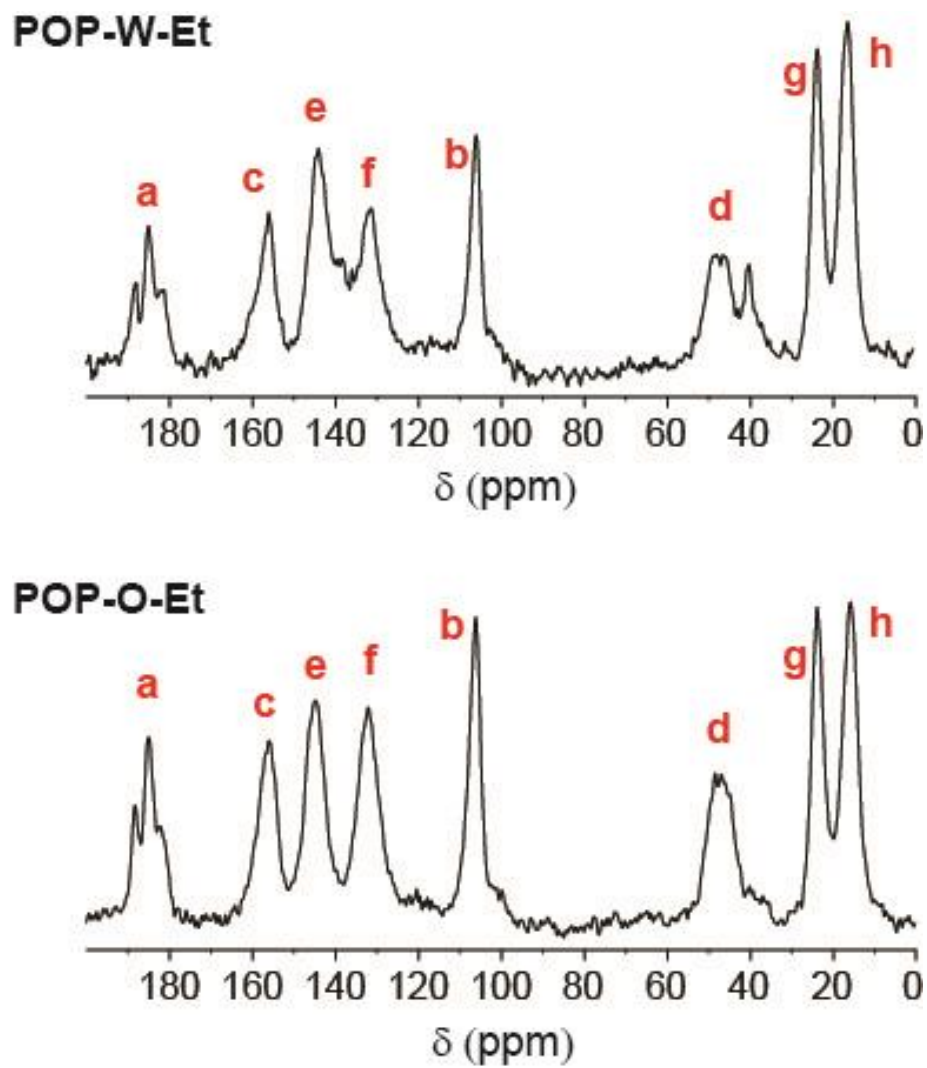


Figure S15 $^{13}\text{C}\{^1\text{H}\}$ SPE MAS spectra of **POP-W-Et** and **POP-O-Et** (up and down, respectively) materials performed at 298 K at a spinning speed of 12.5 kHz with recycle delay of 60 s.

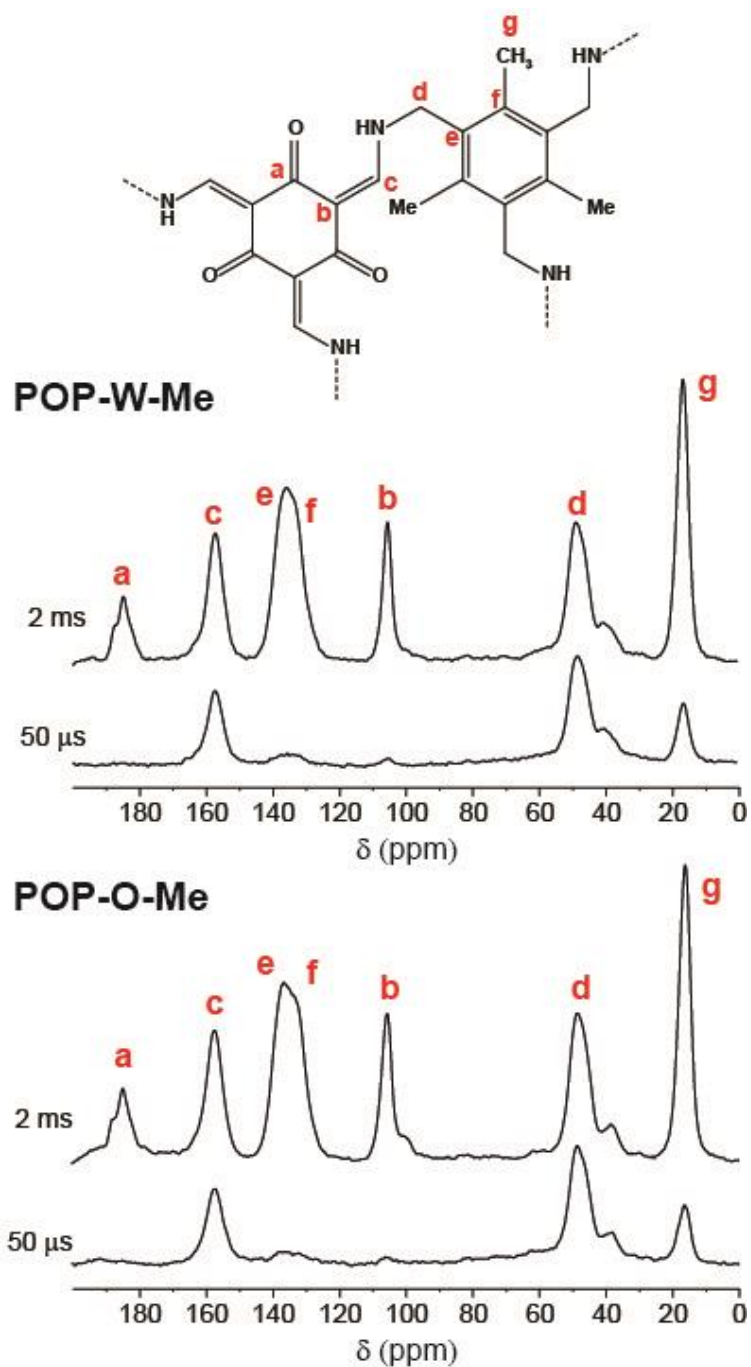


Figure S16. $^{13}\text{C}\{^1\text{H}\}$ CP MAS spectra of **POP-W-Me** and **POP-O-Me** (up and down, respectively) materials performed at 298 K at a spinning speed of 12.5 kHz with contact times of 2 ms and 50 μs . (The samples were treated under high vacuum at 80 $^\circ\text{C}$ for 12 hours before the NMR measurements).

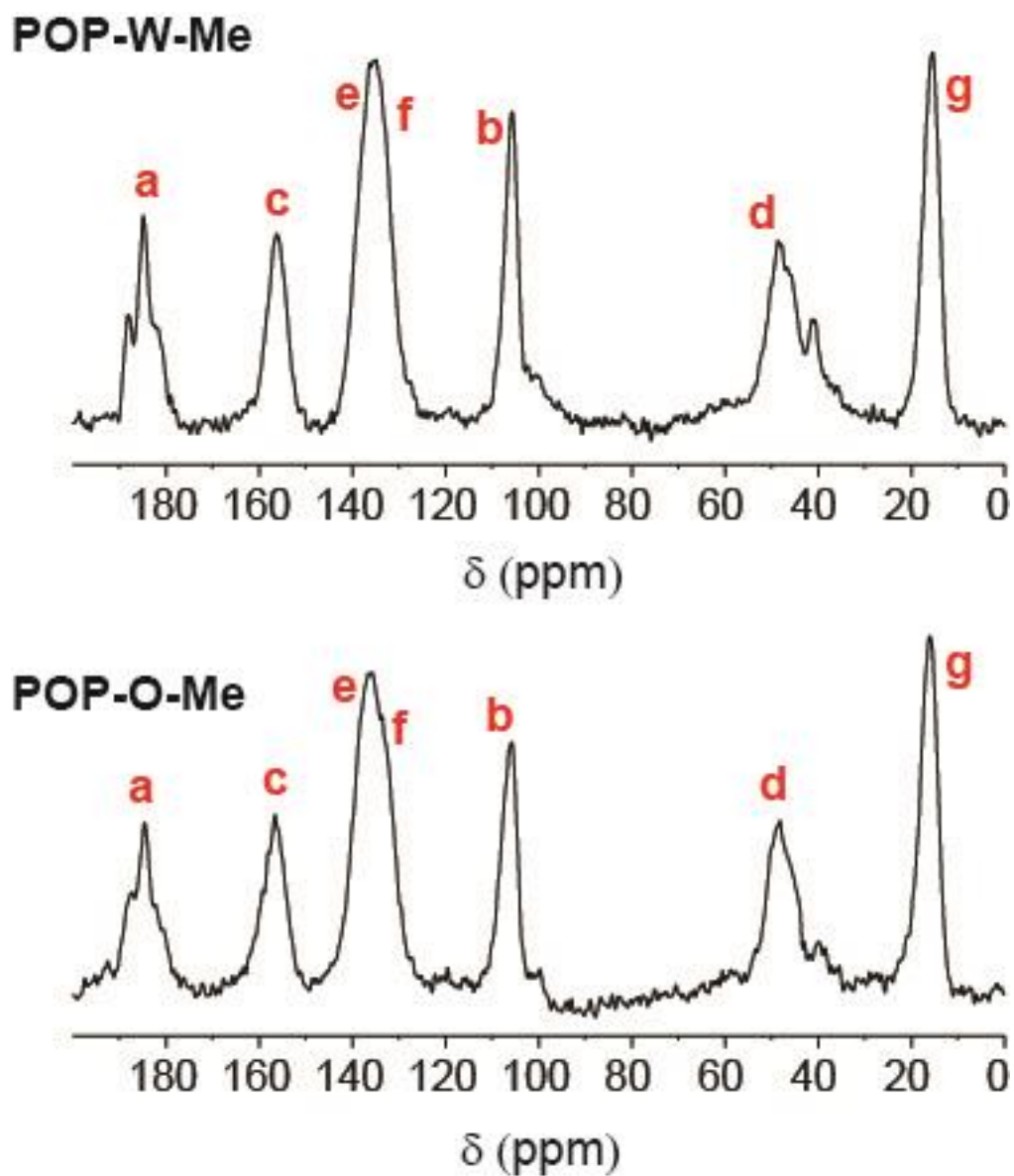


Figure S17. $^{13}\text{C}\{^1\text{H}\}$ SPE MAS spectra of **POP-W-Me** and **POP-O-Me** (up and down, respectively) materials performed at 298 K at a spinning speed of 12.5 kHz with recycle delay of 60 s.

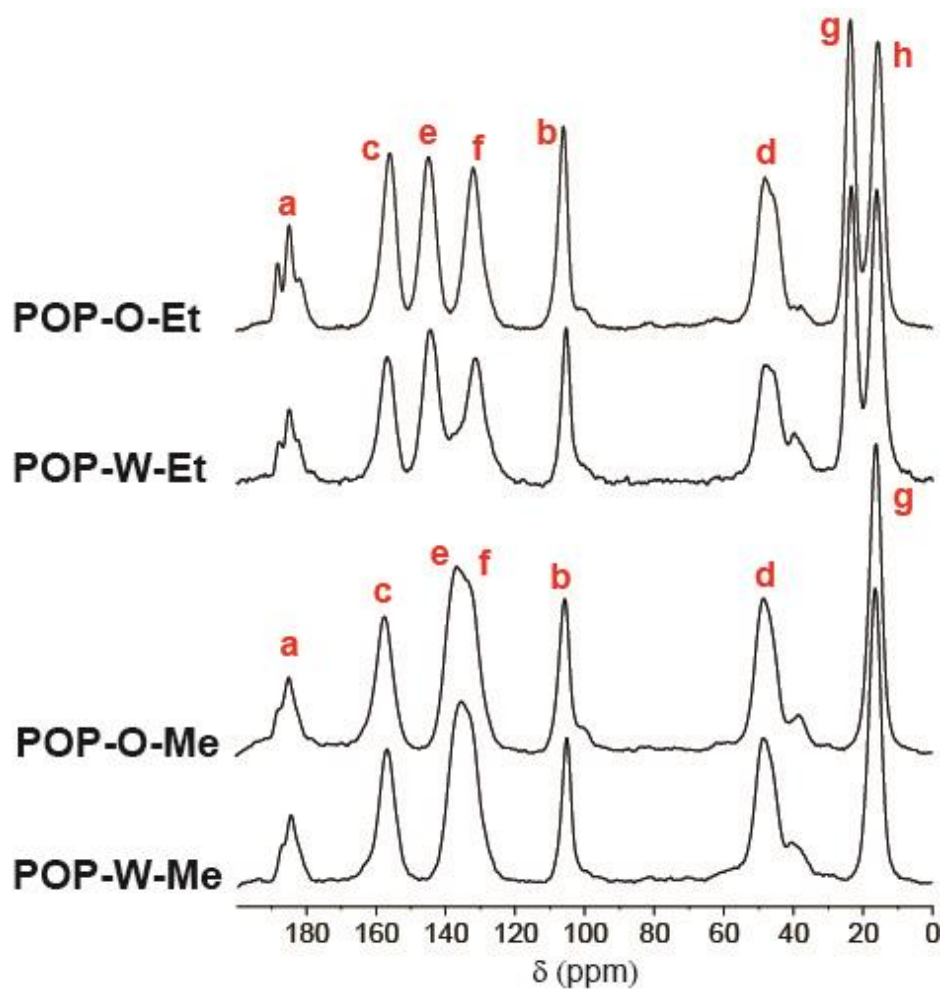


Figure S18. $^{13}\text{C}\{^1\text{H}\}$ CPMAS spectra of materials performed at 298 K at a spinning speed of 12.5 kHz with contact times of 2 ms.

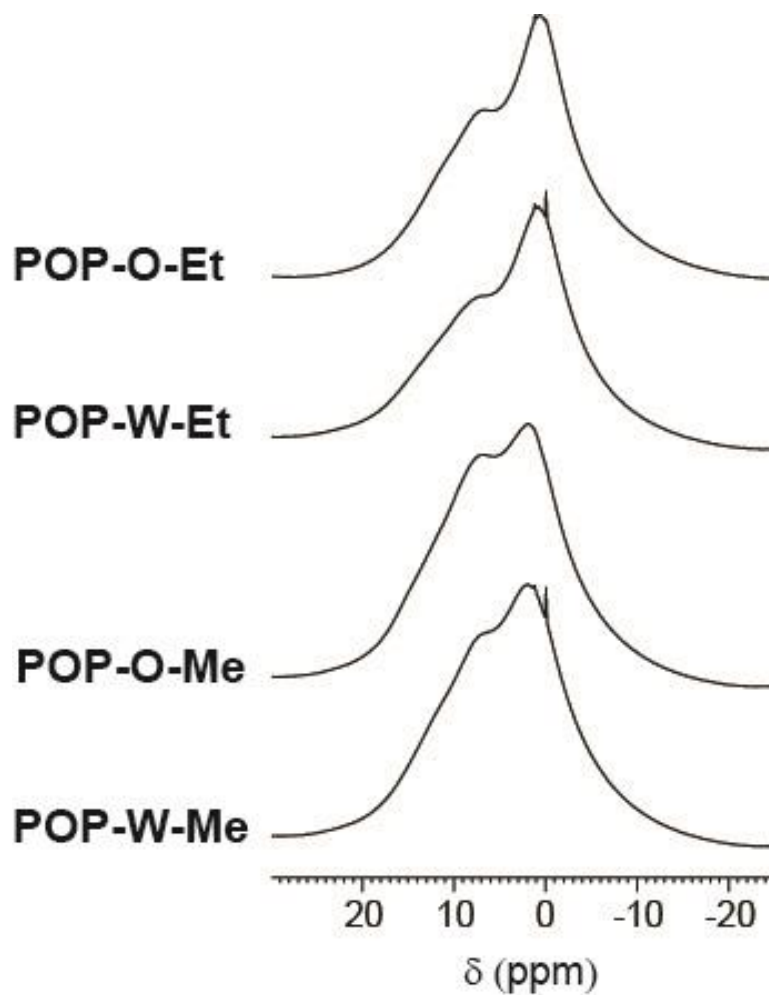
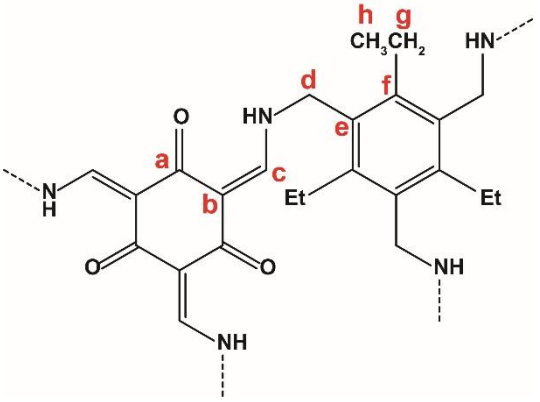
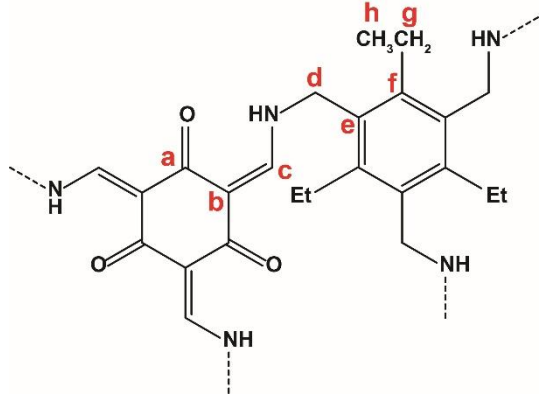


Figure S19. ^1H -MAS spectra of materials performed at 298 K at a spinning speed of 12.5 kHz with a recycle delay of 20 s.

Table S2. ^{13}C chemical shifts from $^{13}\text{C}\{^1\text{H}\}$ CP MAS spectra collected at 7.04 T and 298 K.

POP-O-Et	Assignment	δ (ppm)
	C_a	188.1 184.8 181.9
	C_b	105.9
	C_c	155.8
	C_d	48.0 (45.9)
	C_e	144.7
	C_f	131.9
	C_g	23.5
	C_h	15.6
POP-W-Et	Assignment	δ (ppm)
	C_a	188.0 184.9 182.5
	C_b	105.4
	C_c	156.8
	C_d	48.4 (47.5)
	C_e	144.3
	C_f	131.3
	C_g	23.4
	C_h	16.1

POP-O-Me	Assignment	δ (ppm)
	C_a	187.9 184.6
	C_b	105.5
	C_c	157.2
	C_d	48.5
	C_{e-f}	136.5– 133.2
	C_g	16.2
POP-W-Me	Assignment	δ (ppm)
	C_a	187.6 184.8
	C_b	105.3
	C_c	157.1
	C_d	48.6
	C_{e-f}	135.7
	C_g	16.3

3.6 Powder X-Ray Diffraction Analysis

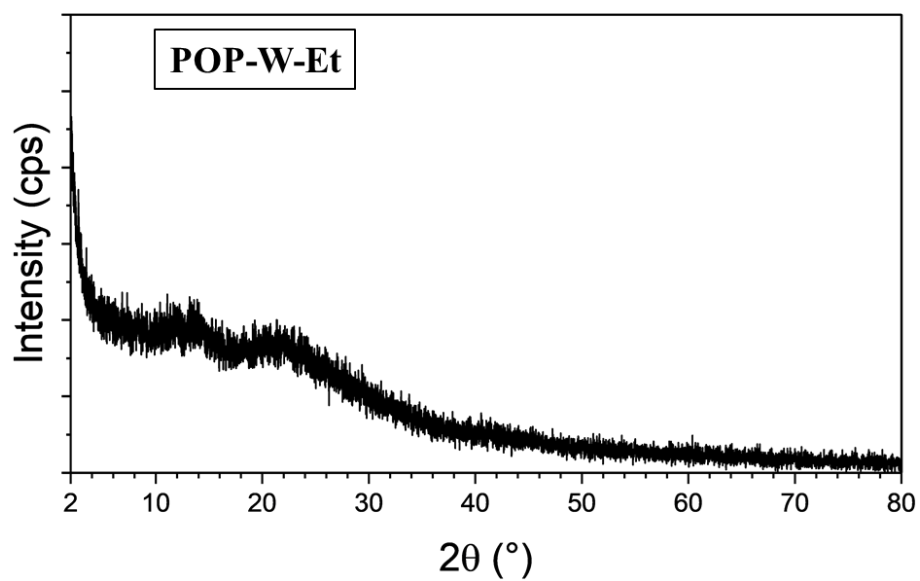


Figure S20 PXR of POP-W-Et

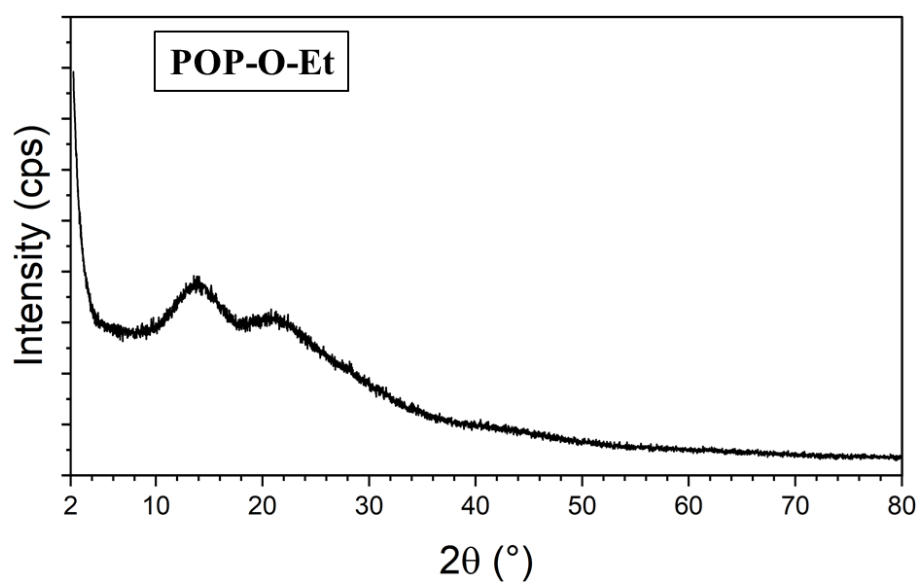


Figure S21 PXR of POP-O-Et

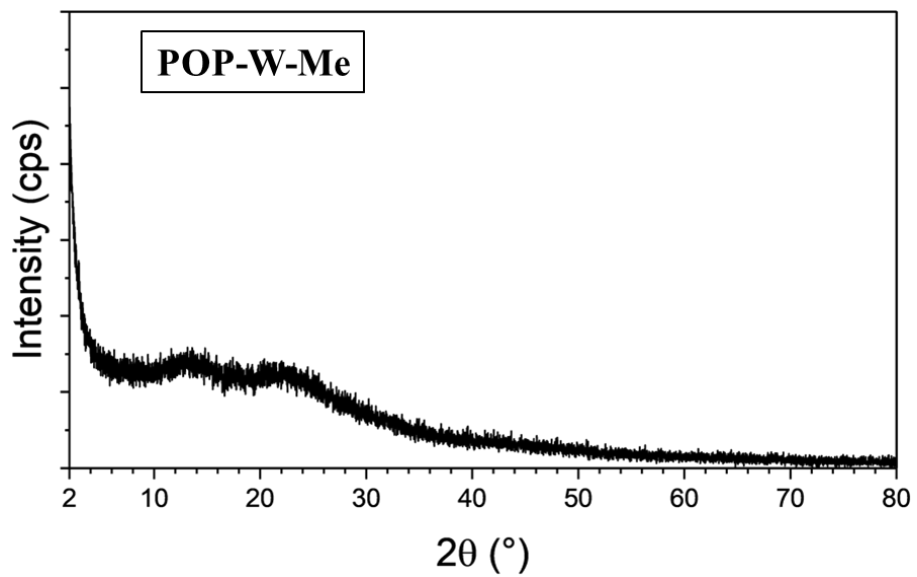


Figure S22 PXR D of POP-W-Me

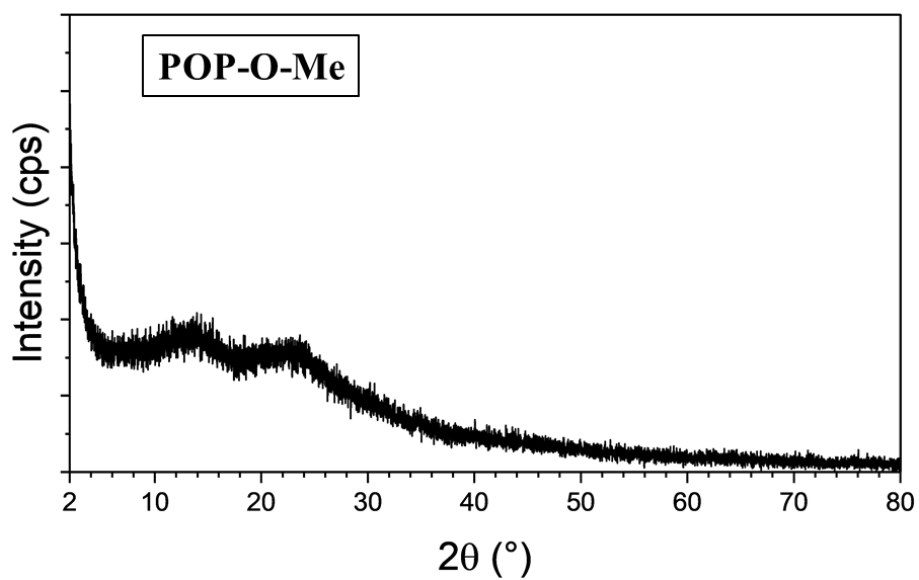
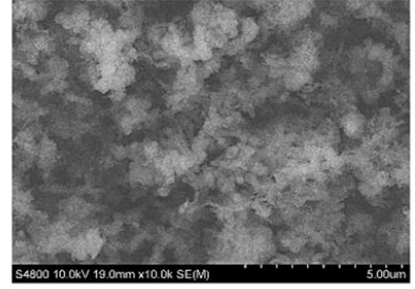
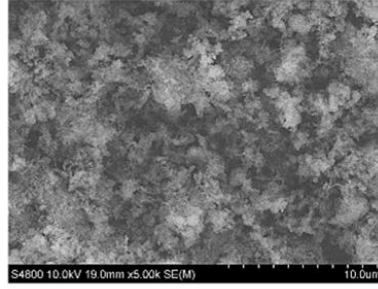
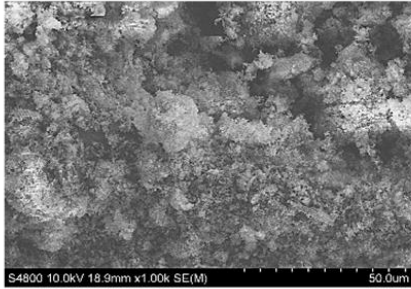


Figure S23 PXR D of POP-O-Me

3.7 Scanning Electron Microscopy Images

POP-W-Me



POP-O-Me

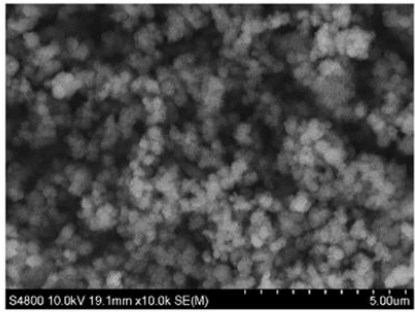
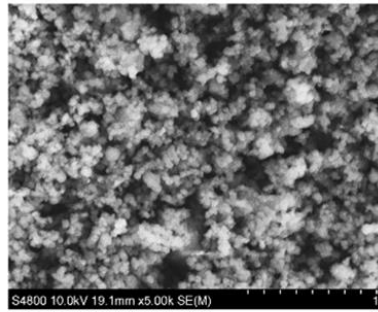
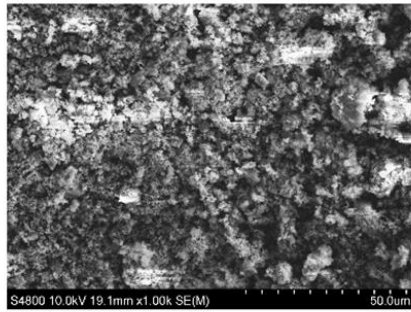
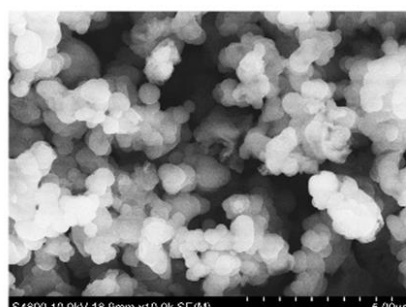
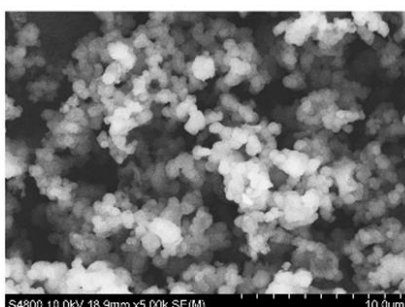
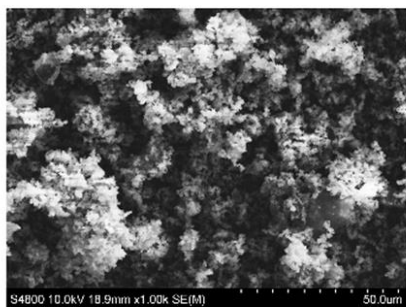


Figure S24 SEM pictures of POP-W-Me and POP-O-Me at different magnifications

POP-W-Et



POP-O-Et

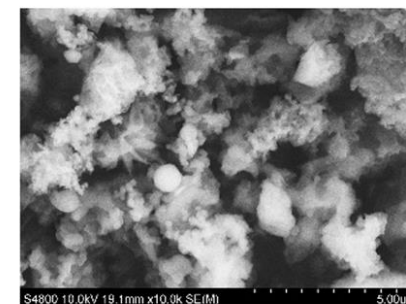
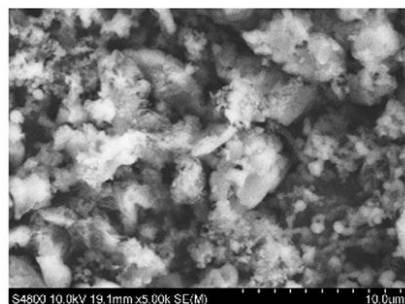
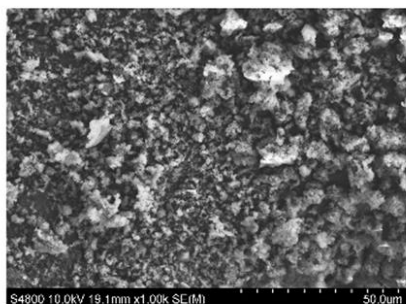


Figure S25 SEM pictures of POP-W-Et and POP-O-Et at different magnifications

4. Gas adsorption studies

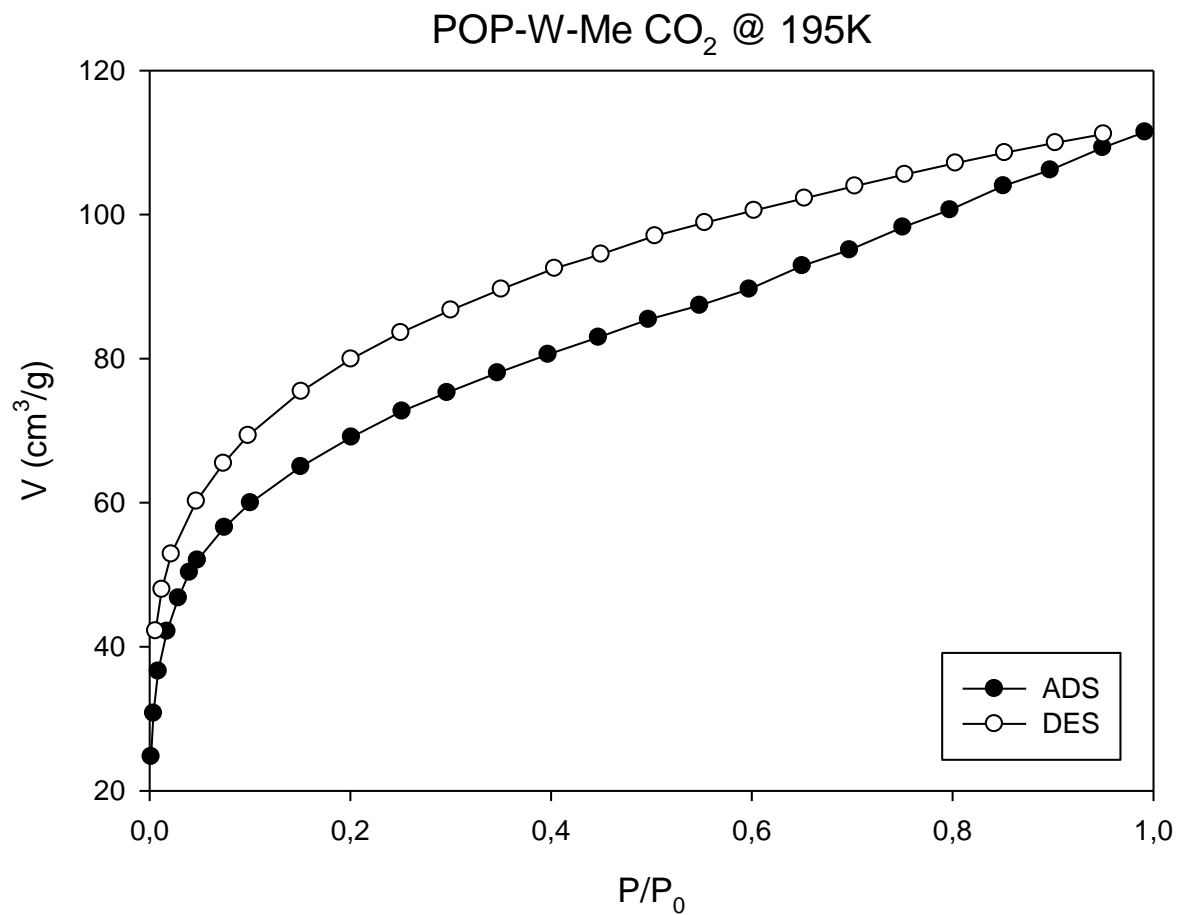


Figure S26 CO₂ Adsorption-Desorption curve of POP-W-Me at 195 K.

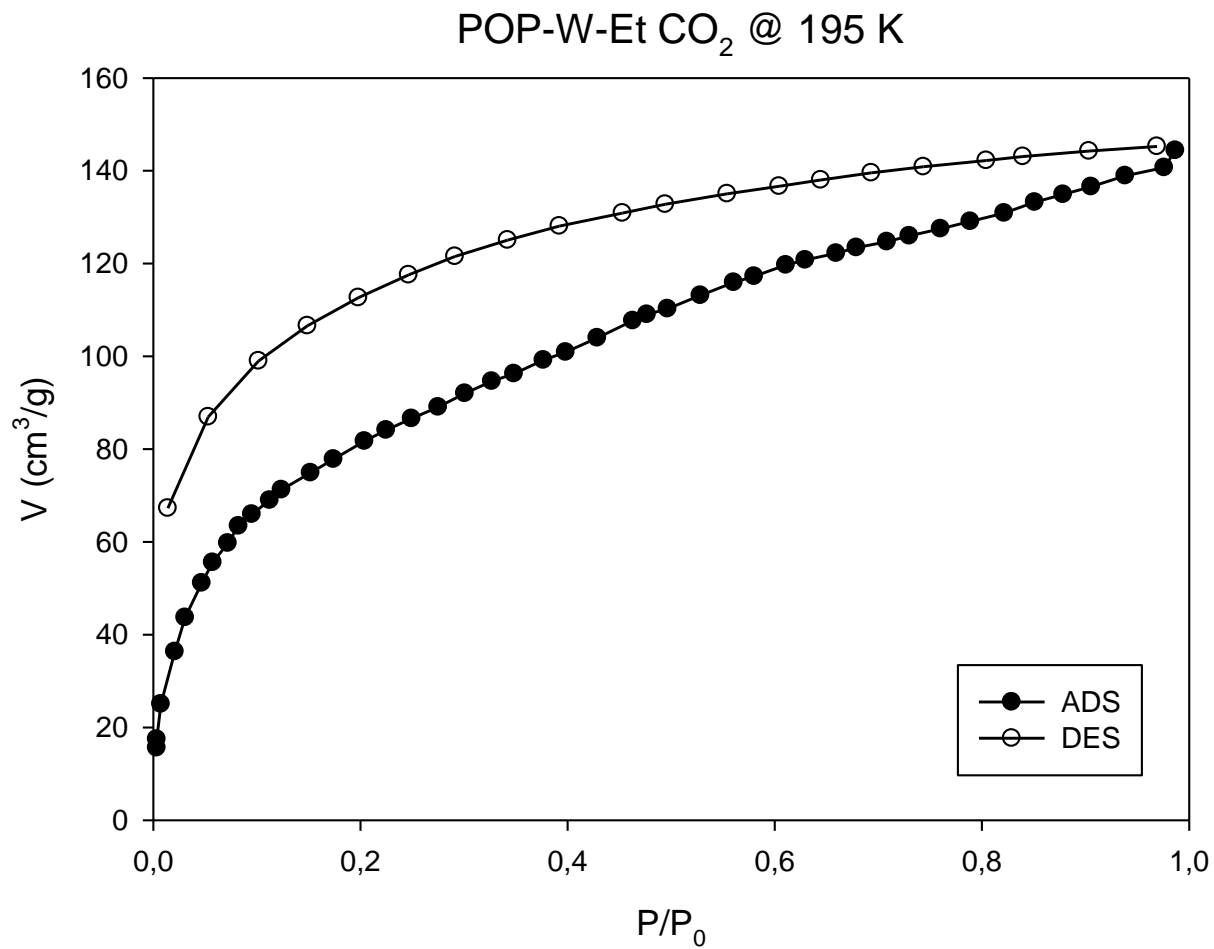


Figure S27 CO₂ Adsorption-Desorption curve of POP-W-Et at 195 K.

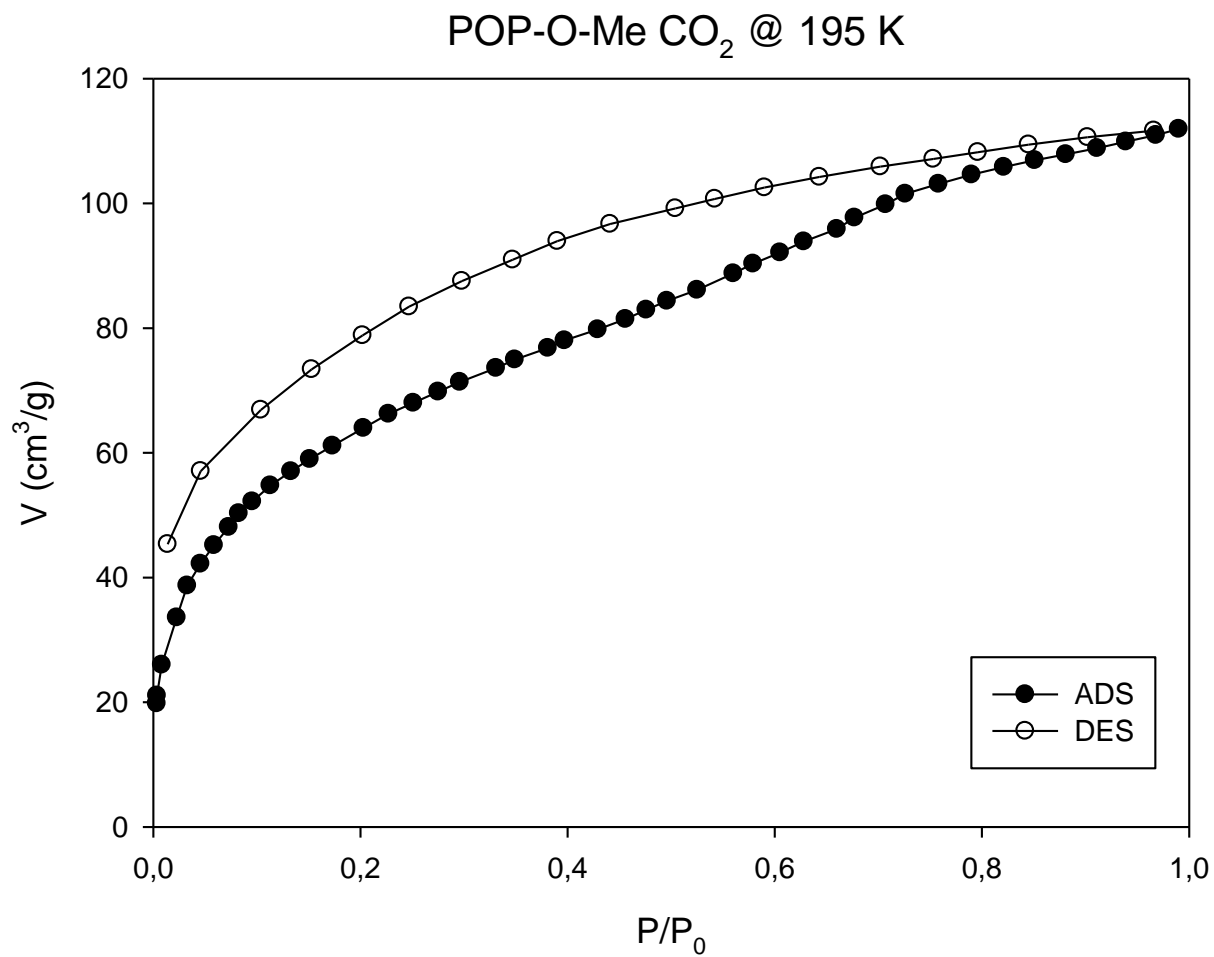


Figure S28 CO₂ Adsorption-Desorption curve of POP-O-Me at 195 K.

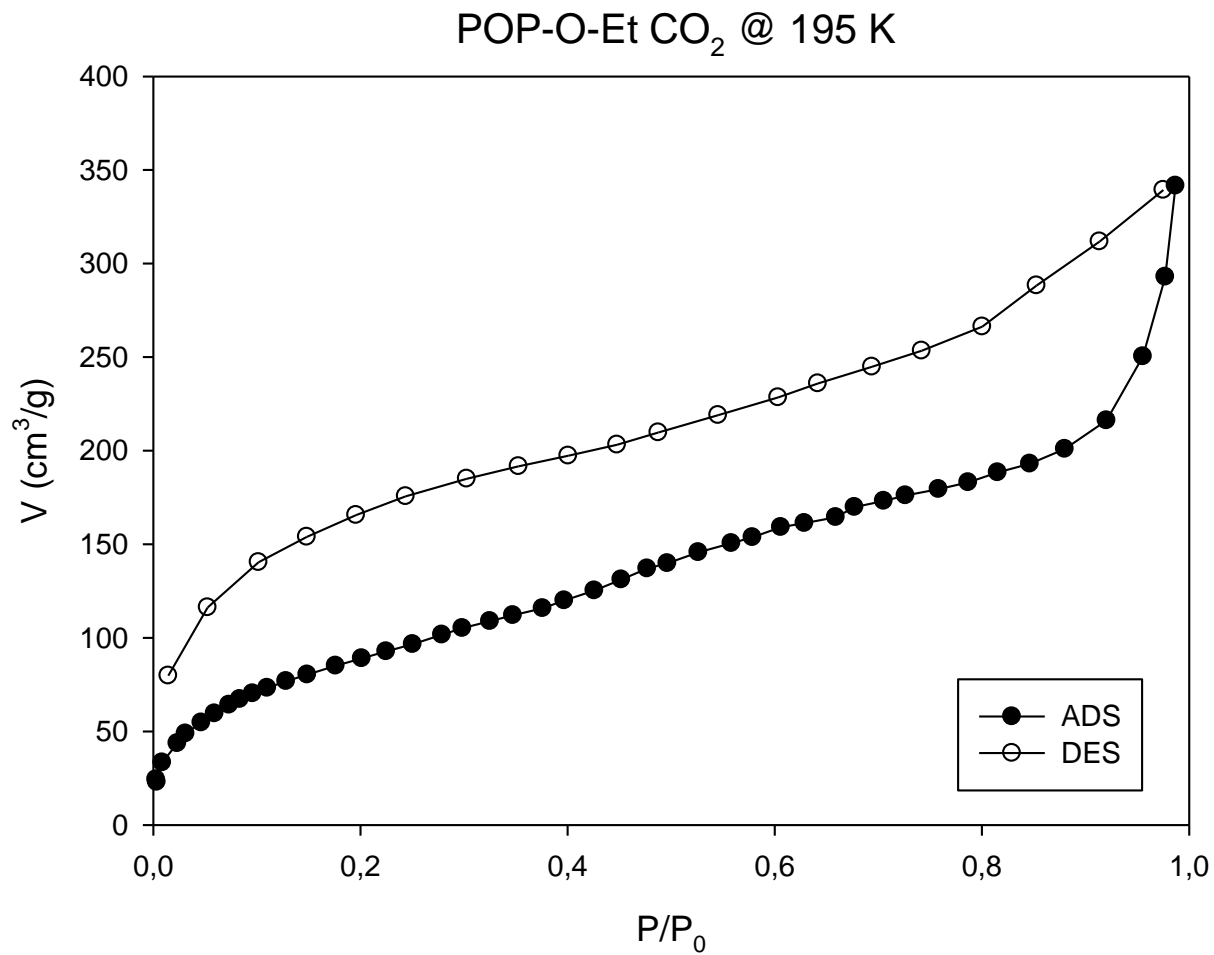


Figure S29 CO₂ Adsorption-Desorption curve of POP-O-Et at 195 K.

POP-W-Me CO₂ @ 273 K

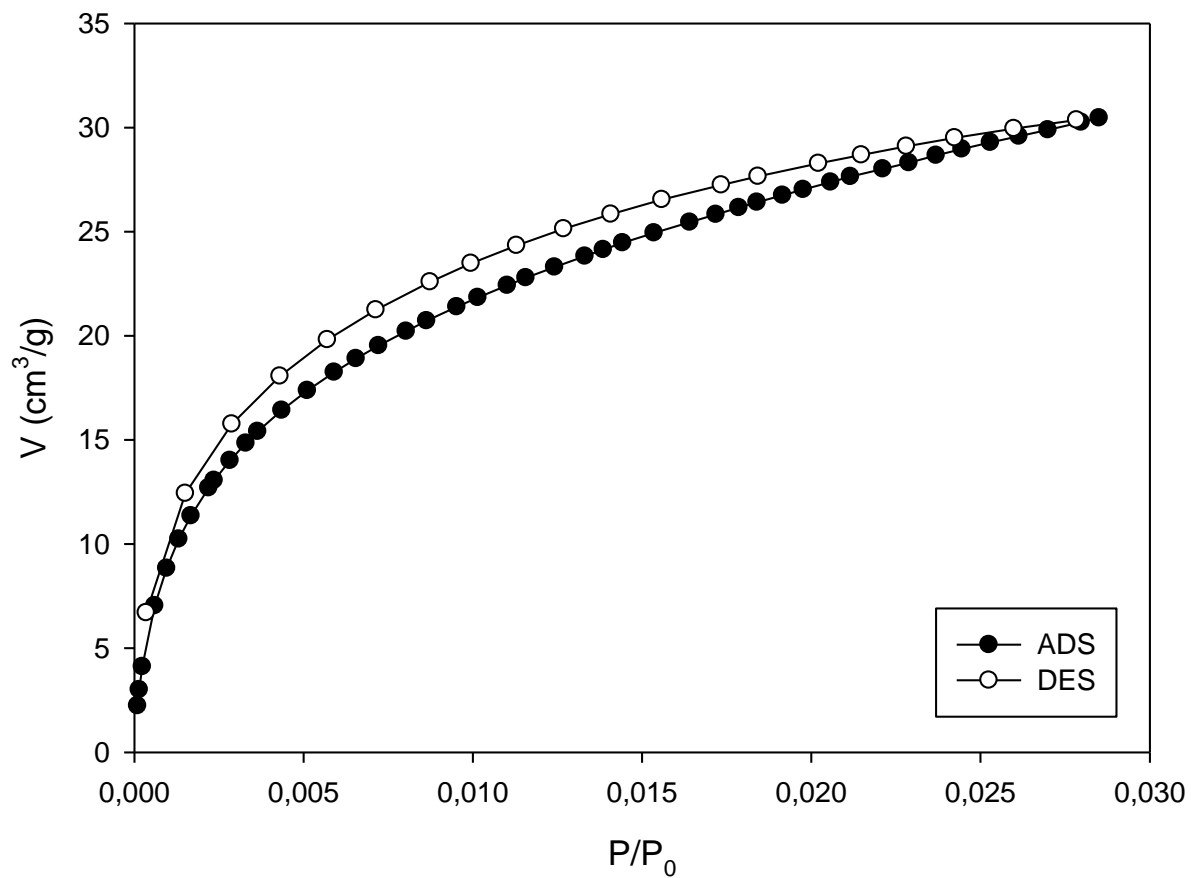


Figure S30 CO₂ Adsorption-Desorption curve of POP-W-Me at 273 K.

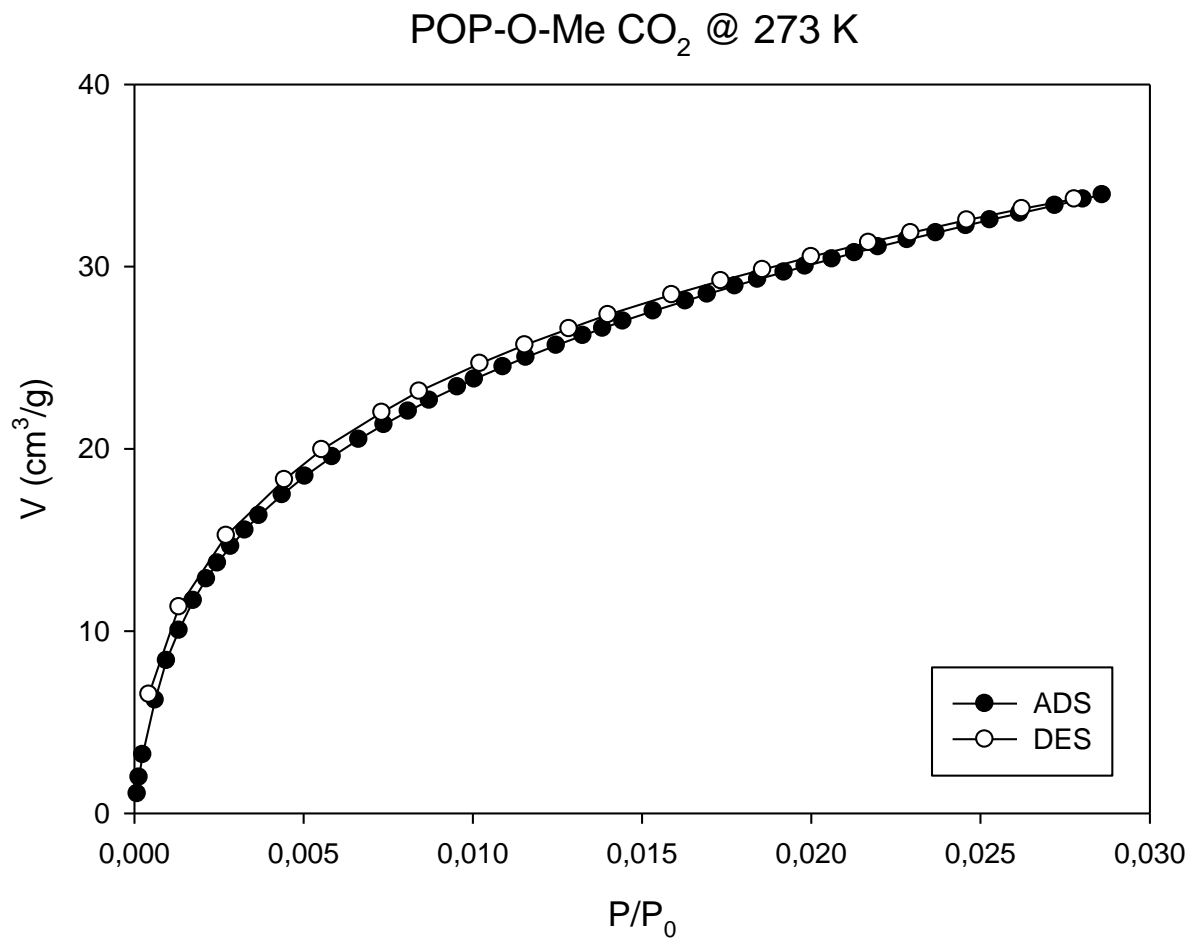


Figure S31 CO₂ Adsorption-Desorption curve of POP-O-Me at 273 K.

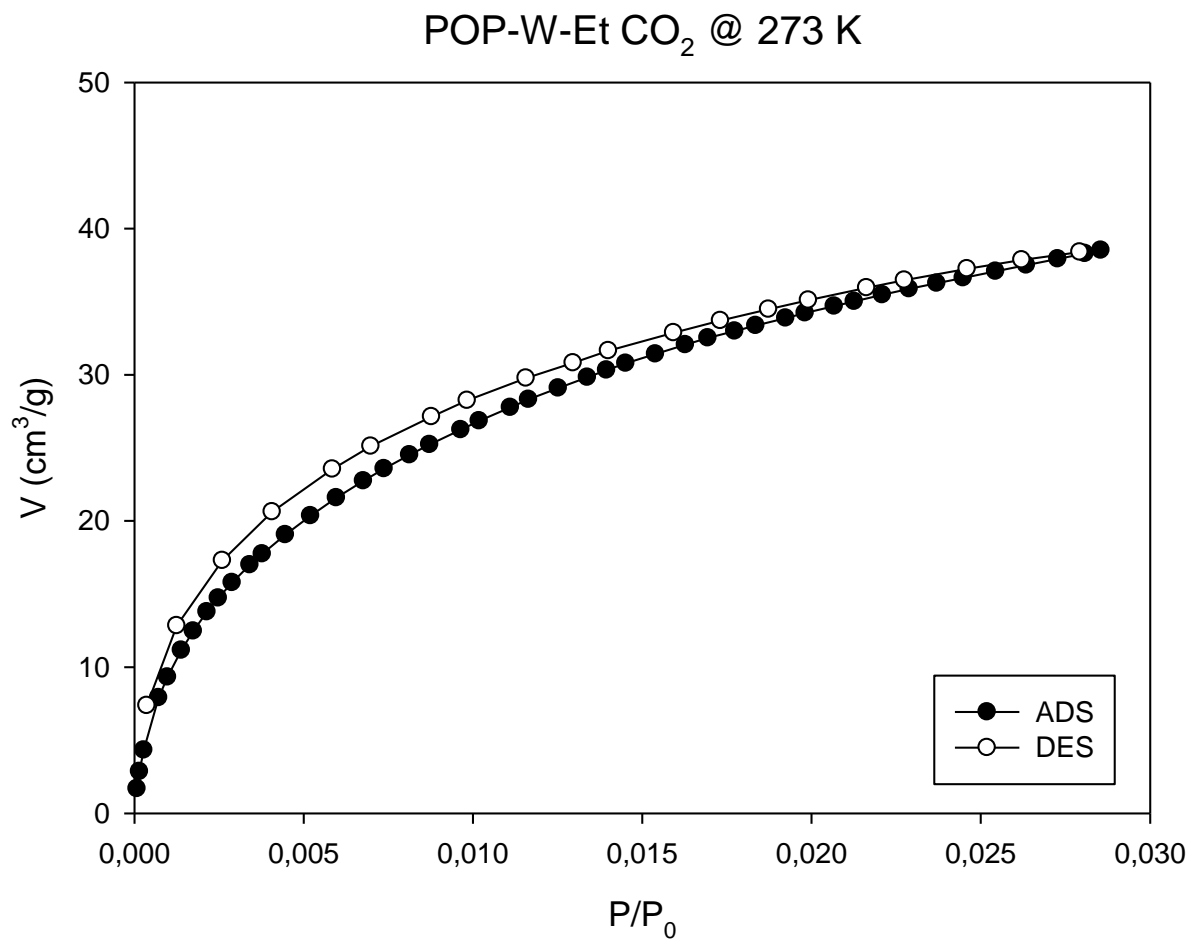


Figure S32 CO₂ Adsorption-Desorption curve of POP-W-Et at 273 K.

POP-O-Et CO₂ @ 273 K

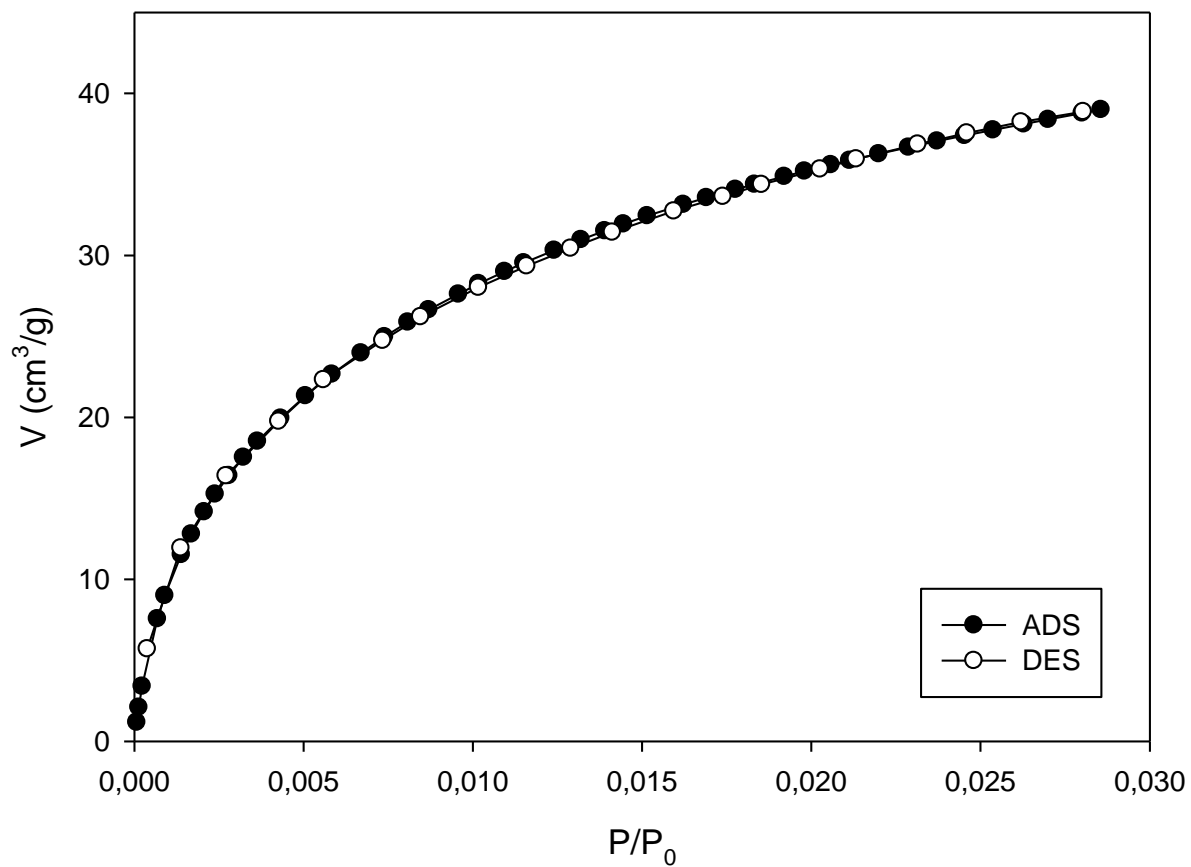


Figure S33 CO₂ Adsorption-Desorption curve of POP-O-Et at 273 K.

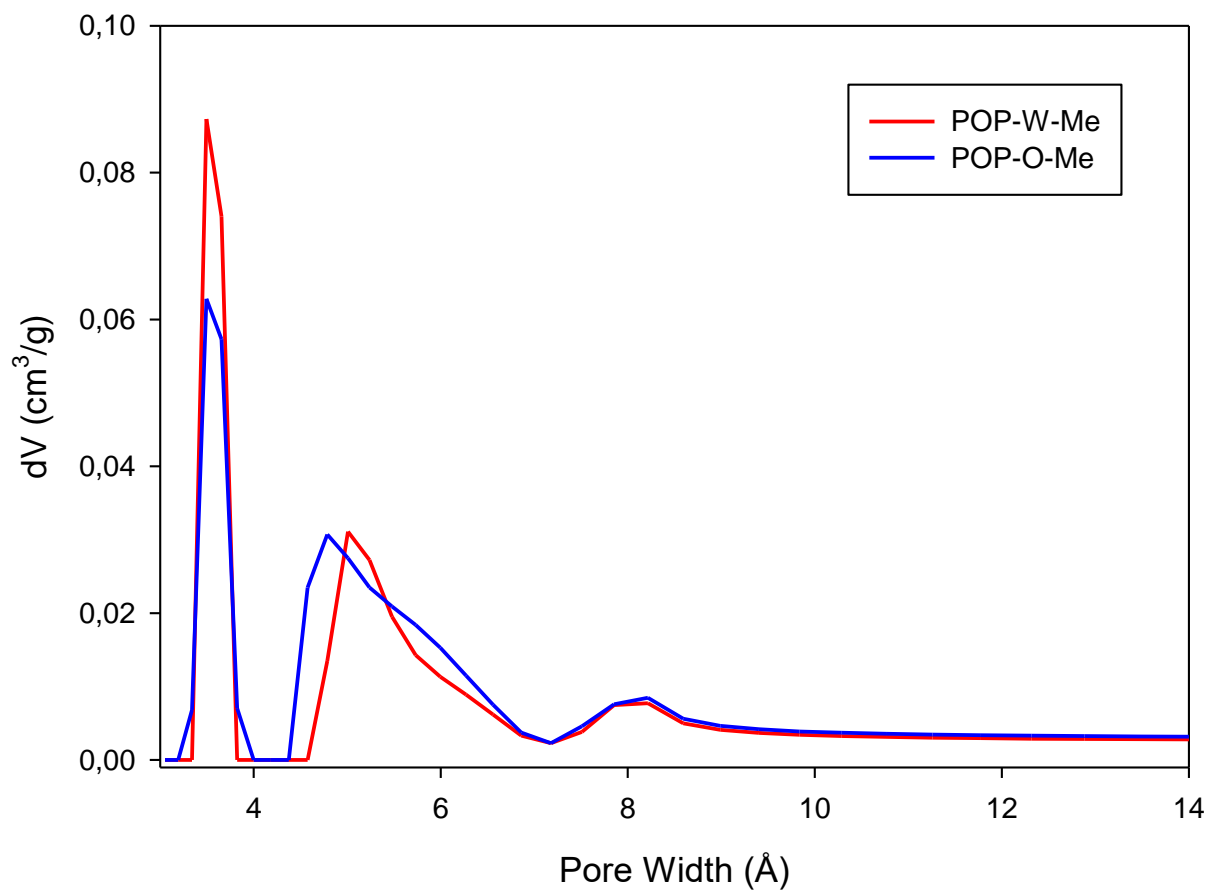


Figure S34 PSD of POP-W-Me and POP-O-Me (red and blue line, respectively)

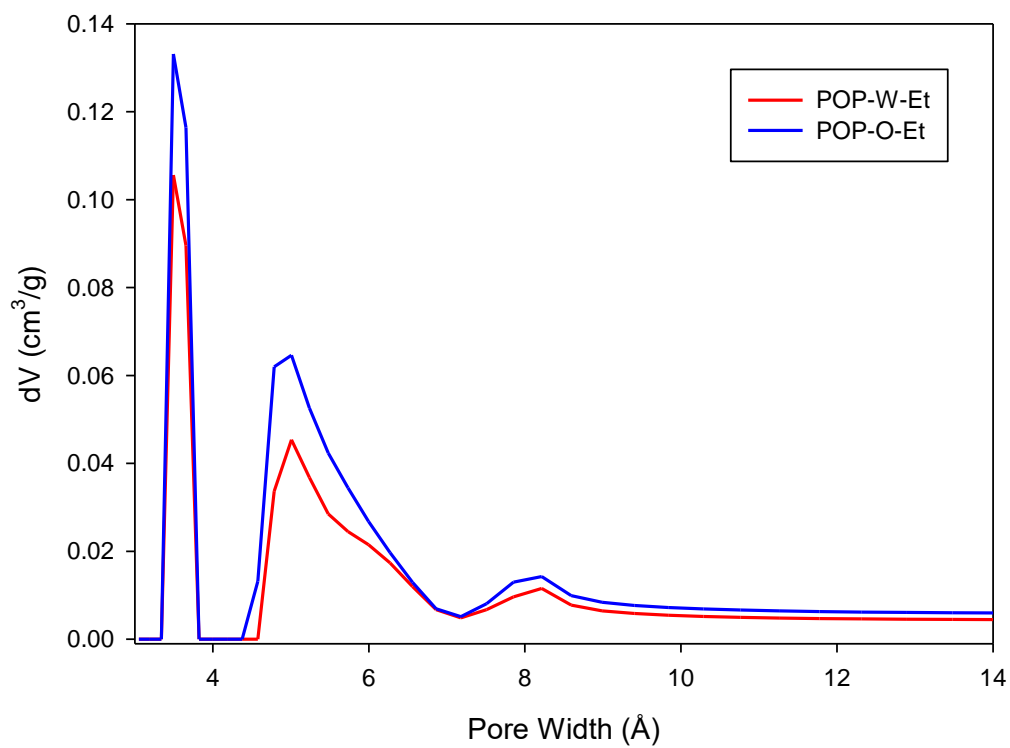


Figure S35 PSD of POP-W-Et and POP-O-Et (red and blue line, respectively)

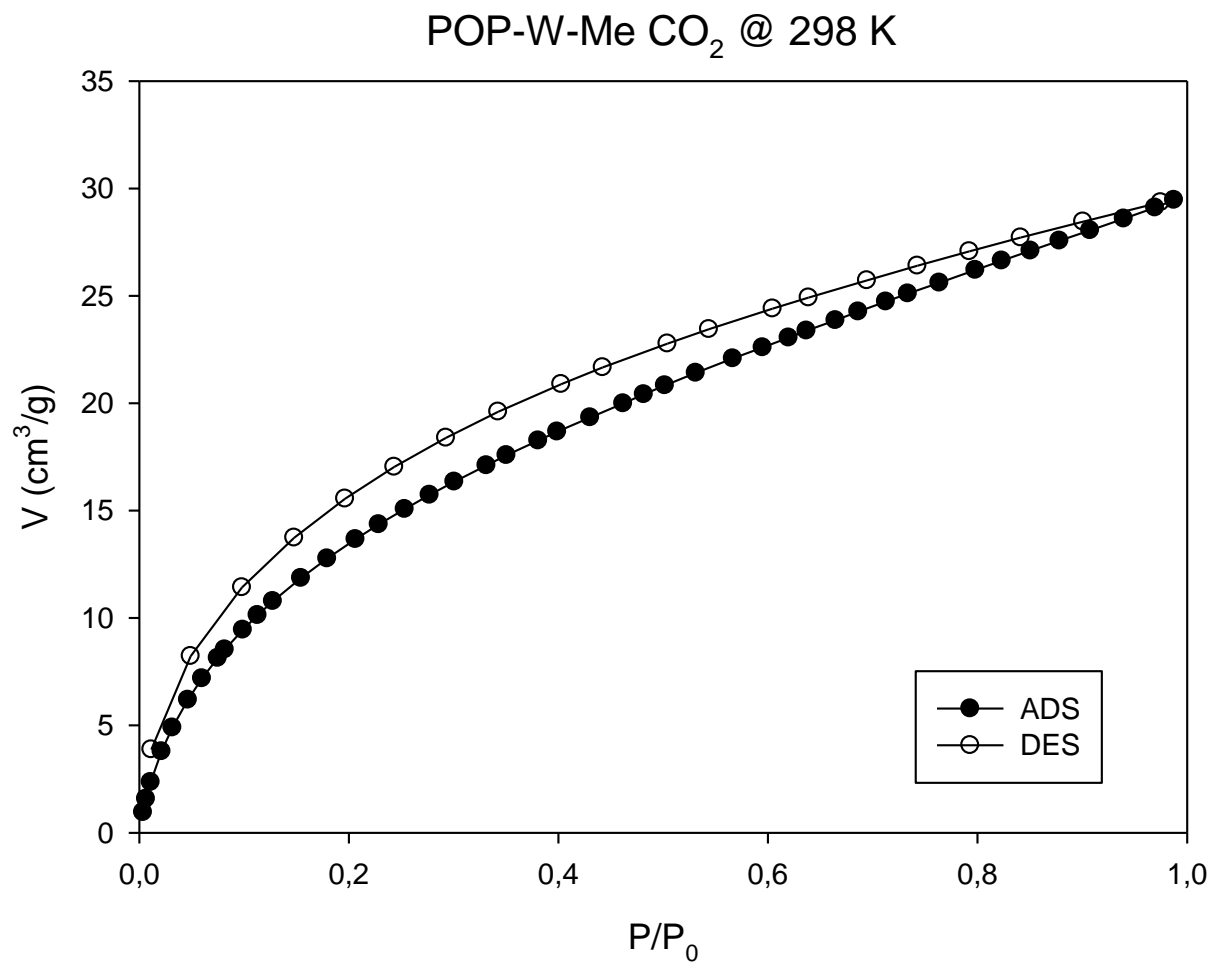


Figure S36 CO₂ Adsorption-Desorption curve of POP-W-Me at 298 K.

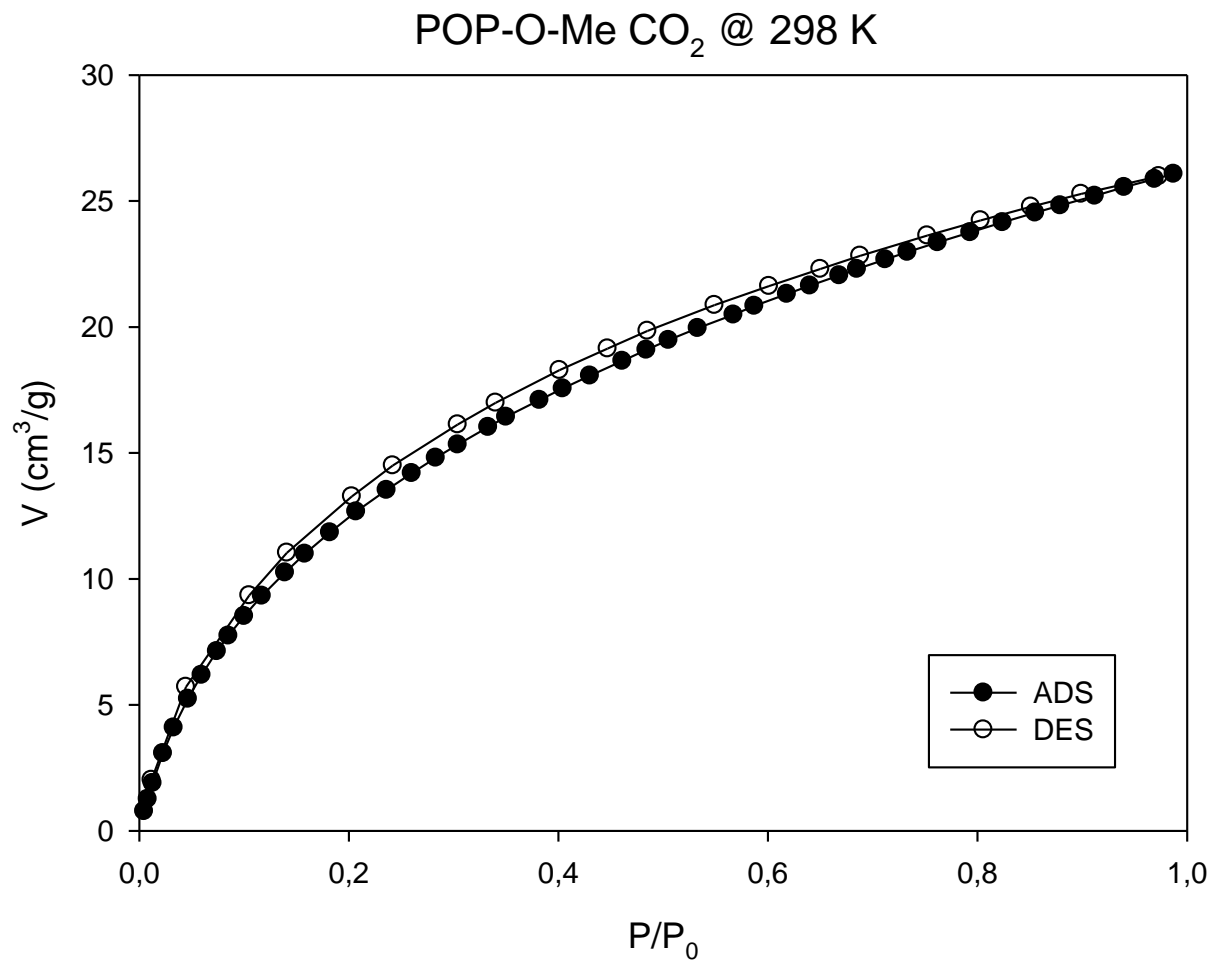


Figure S37 CO₂ Adsorption-Desorption curve of POP-O-Me at 298 K.

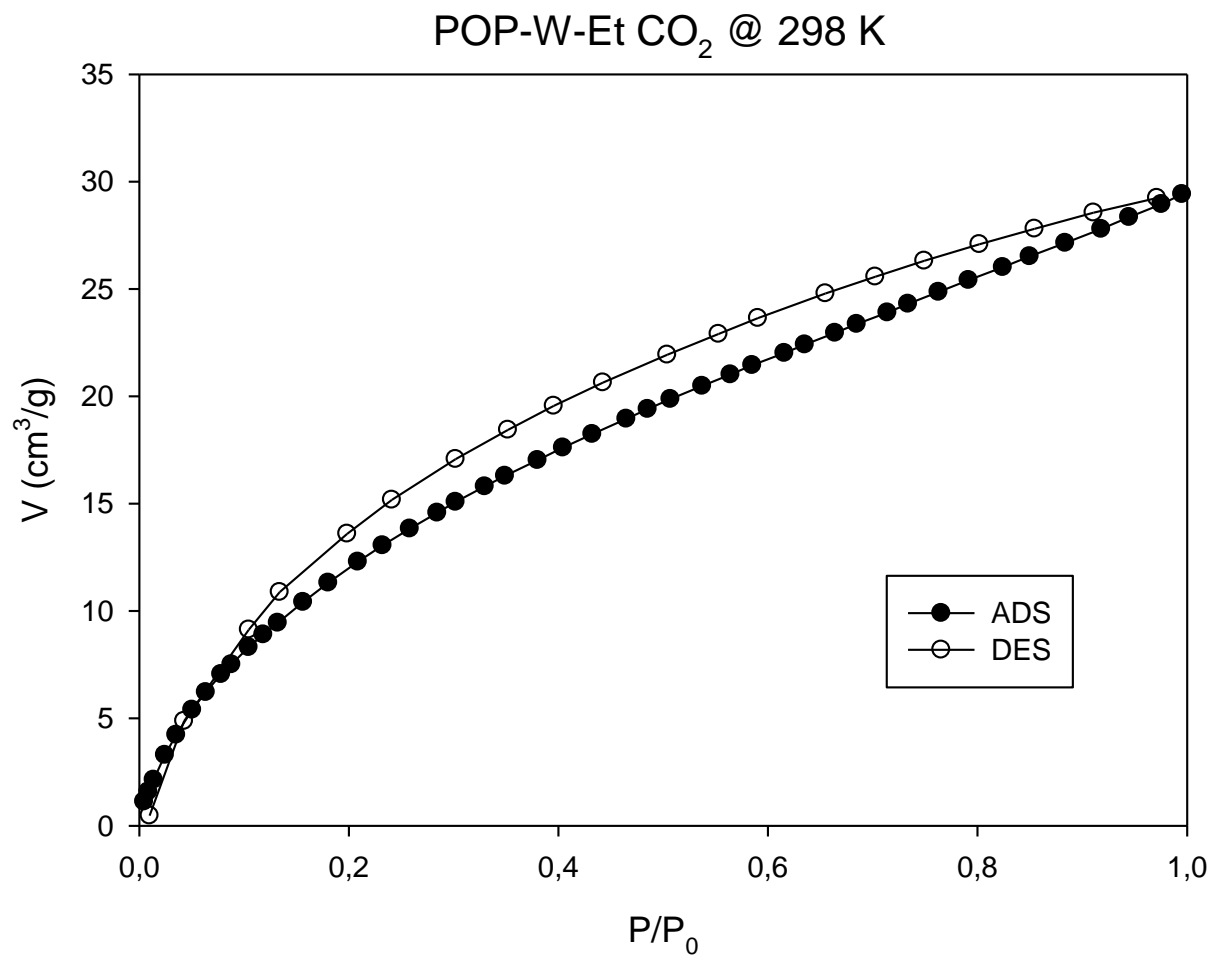


Figure S38 CO₂ Adsorption-Desorption curve of POP-W-Et at 298 K.

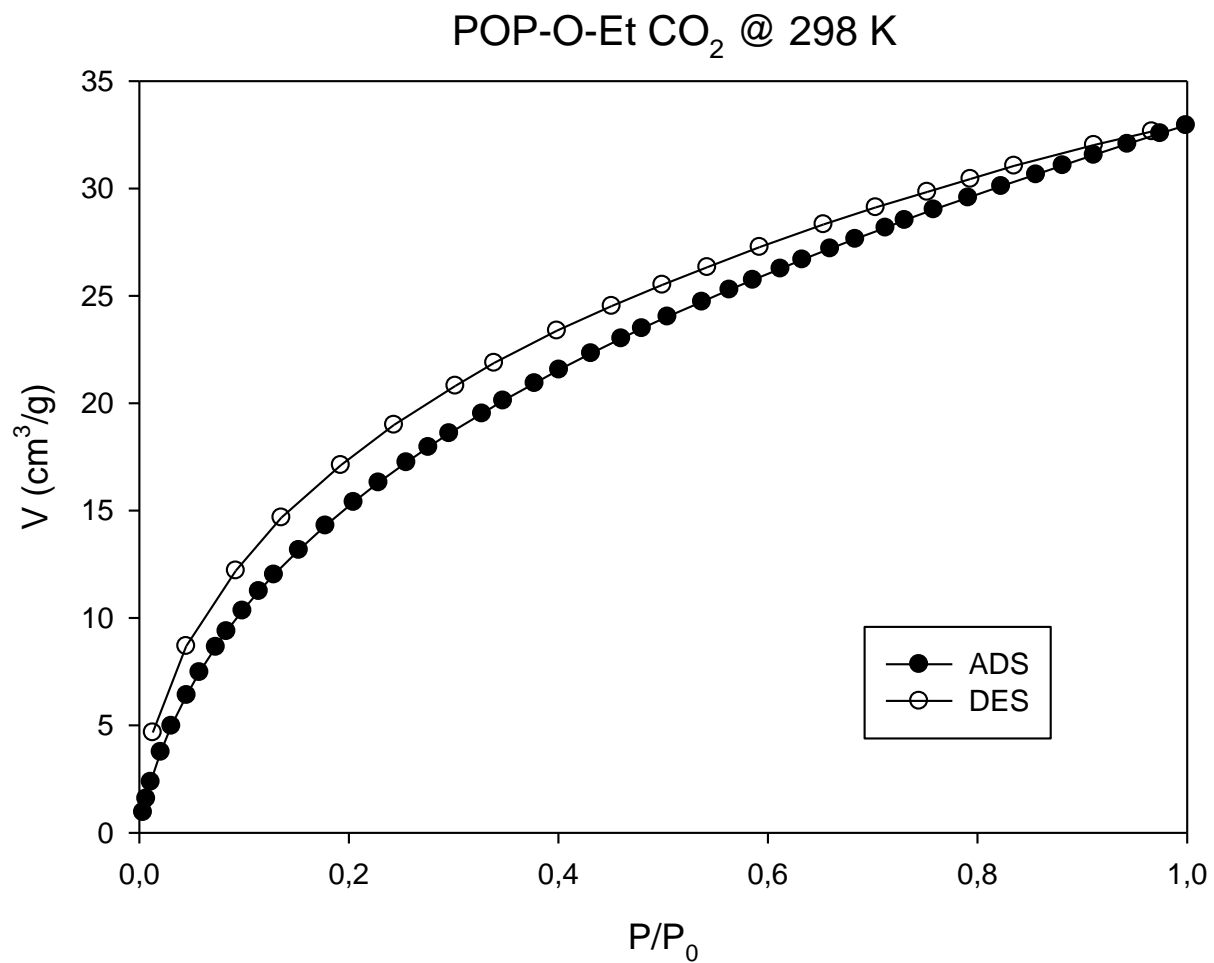


Figure S39 CO₂ Adsorption-Desorption curve of POP-O-Et at 298 K.

Table S3. Comparison with other studies on CO₂-philic POPs synthesized in water or water:ethanol mixture, in either presence or absence of catalysts (or additives).

POP	Solvent	Catalyst/additive	T°C	Time (days)	Yield %	CO ₂ uptake (mmol g ⁻¹)	S _{ABET} (m ² g ⁻¹)	Ref
POP-W-Et	H ₂ O	//	70	3	90	1.70 ^a	389 ^c	*
POP-W-Me	H ₂ O	//	70	3	93	1.52 ^a	348 ^c	*
PI(TAPB-PMA)	H ₂ O (HTP)	AcOH	200	1	n.a.	1.65 ^a	207 ^c	S4
SMPA-TPA POP	H ₂ O	AcOH	60/120	3	76/72	1.34/1.29 ^b	680/513 ^d	S5
MPA-TPA POP	H ₂ O/EtOH (2/1, v/v)	AcOH	120	3	90	1.49 ^b	931 ^d	S5
HAzo-POP-3	H ₂ O	NaNO ₂	0–5	<1	97	1.70 ^a	418 ^d	S6

CO₂ uptake obtained from a) adsorption isotherms at 273 K (1 bar) or b) gravimetric CO₂ uptake measured on TGA at 298K (1 bar); S_{ABET} values obtained using c) CO₂ at 195 K or d) N₂ at 77 K. HTP: hydrothermal polymerisation; n.a.: not available. * This work.

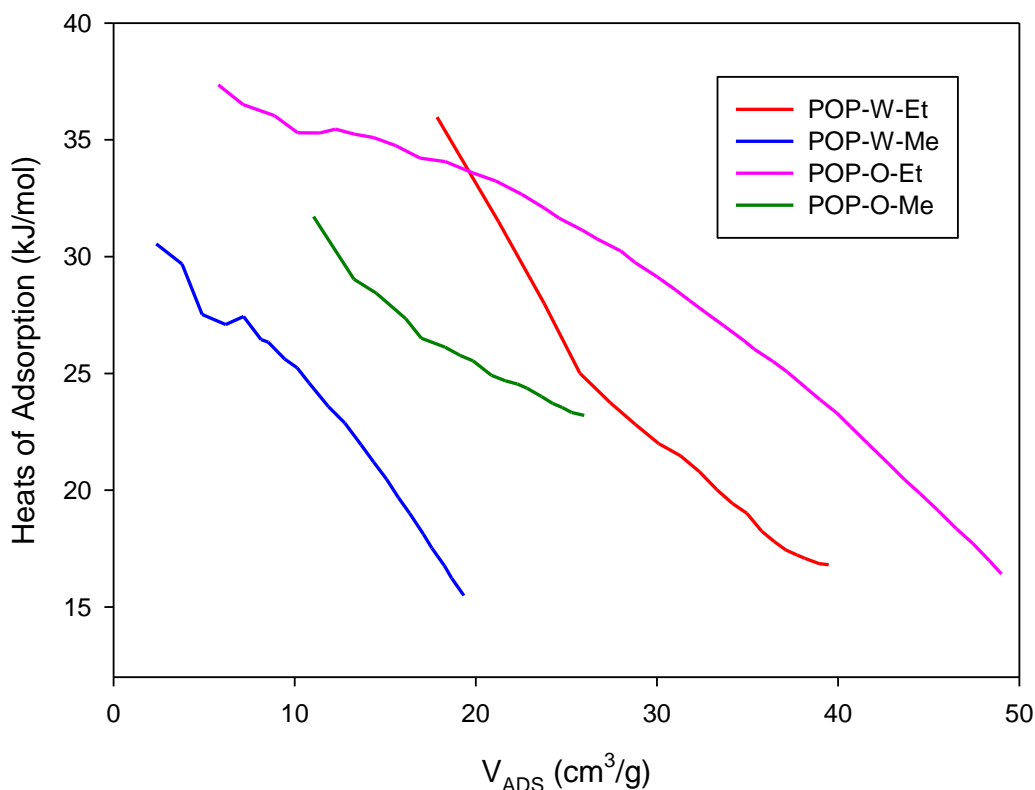


Figure S40 Heats of adsorption of POPs

5. References

- S1** R. Mobili, S. La Cognata, M. Monteleone, M. Longo, A. Fuoco, S. A. Serapian, B. Vigani, C. Milanese, D. Armentano, J. C. Jansen and V Amendola, *Chem. Eur. J.*, **2023**, *29*, e202301437.
- S2** R.L. Greenaway, V. Santolini, M.J. Bennison, B.M. Alston, C.J. Pugh, M.A. Little, M. Miklitz, E.G.B. Eden-Rump, R. Clowes, A. Shakil, H. J. Cuthbertson, H. Armstrong, M. E. Briggs, K. E. Jelfs, A. I. Cooper, *Nat. Commun.* **2018**, *9*(1), 2849.
- S3** J. H. Chong, M. Sauer, B. O. Patrick, M. J. MacLachlan, *Org. Lett.*, **2003**, *5*(21), 3823–3826.
- S4** a) M. Lahnsteiner, M. Caldera, H. M. Moura, D. A. Cerron-Infantes, J. Roeser, T. Konegger, A. Thomas, J. Menche, and M. M. Unterlass, *J. Mater. Chem. A* **2021**, *9*, 19754–19769; b) B. Baumgartner, M. Puchberger and M. Unterlass, *Polym. Chem.* **2015**, *6*, 5773–5781
- S5** D. Luo, T. Shi, Q.-H. Li, Q. Xu, M. Strømme, Q.-F. Zhang, C. Xu, *Angew. Chem. Int. Ed.* **2023**, *62*, e202305225
- S6** G. Ji, Z. Yang, H. Zhang, Y. Zhao, B. Yu, Z. Ma, and Z. Liu, *Angew. Chem. Int. Ed.* **2016**, *55*, 9685–9689